Dielectric Measurement and Analysis of Ultrastable PMMA Glass

by

Zhaohui Cai

A thesis
presented to the University of Waterloo
in fulfillment of the
thesis requirement for the degree of
Master of Science
in
Physics - Nanotechnology

Waterloo, Ontario, Canada, 2021

Author's Declaration

I hereby declare that I am the sole author of this thesis. This is a true copy of the thesis, including any required final revisions, as accepted by my examiners.

I understand that my thesis may be made electronically available to the public.

Abstract

A stable glass, distinguished from an ordinary glass, has phenomenal characteristics such as a high density and a high kinetic stability. In this project, stable glasses of poly(methylmethacrylate) (PMMA) are produced by physical vapor deposition (PVD), and the dielectric responses of the vapor-deposited PMMA glasses are measured at 1 kHz with a high precision capacitance bridge. Measurements of the dielectric loss and storage have been done by heating and cooling the vapor-deposited PMMA glasses, where the heating and cooling cycles are used to rejuvenate the vapor-deposited PMMA glasses and to directly compare stable and nominally rejuvenated glasses. A noticeable suppression in β relaxation peak could be observed in the dielectric loss curve for vapor-deposited glasses (stable glasses) as compared to that for rejuvenated glasses (ordinary glasses). This finding implies that the glass stability essentially influences the dielectric relaxation.

Acknowledgements

First of all, I would like to express my immense thanks to my supervisor Dr. James Forrest. His guidance and encouragement helped me carry out my research project in the past two years of my master's studies. I would also like to thank my other committee members, Mark Matsen and Dmitry Pushin for their kind and brilliant suggestions.

I would also like to express my sincere appreciation to our group members, Michael Thees, Adam Raegen, Junjie Yin and Tiana Trumpour for their invaluable support and help.

Lastly, I would like to express my deep thanks to my parents for their continuous help in my life.

Dedication

This is dedicated to the one I love.

Table of Contents

List of Figures

List of Tables

Chapter 1

Introduction

1.1 Polymers

A polymer is a long-chain molecule consisting of many repeating units called monomers, which are linked to each other through covalent bonds [7]. Homopolymer is a polymer of one kind of monomer, while heteropolymer is made up with more than one kind of monomer [8]. The number of monomers in a polymer chain can often be determined by looking at a degree of polymerization (N) that is a ratio of the molecular weight of a polymer (M) to the molecular weight of a monomer (M_{mon}):

$$N = \frac{M}{M_{mon}} \tag{1.1}$$

A relatively low molecular weight polymer with $N \leq 20$ (called an oligomer) is generally considered as a favorable choice for producing a stable vapor-deposited glass [9].

Any kind of polymer product can be synthesized from a process called polymerization by grouping monomers via a variety of chemical reactions to form a polymer chain. Gen-

erally, the process is categorized into two methods: step-growth and chain-growth. In the step-growth polymerization, monomers react in a step-wise manner to form a long polymer chain [10]. Formations of polyamides and polyesters are typical examples of this polymerization process. In the chain-growth polymerization, monomers are simply added onto the active sites on a growing polymer chain. Initiation, propagation, and termination are three successive stages, involved in the chain-growth polymerization. A typical example of chain-growth polymerization is the formation of polyethylenes. With conventional and current synthetic techniques, it is almost impossible to synthesize a polymer product with all its polymer chains of the same molecular weight [11]. Each polymer product's chains generally have different molecular weights and therefore, an average molecular weight is used to characterize a polymer product. The average molecular weight of polymer product is commonly expressed in two ways: number average molecular weight and weight average molecular weight. The number average molecular weight is the ratio of the total molecular weight to the total number of all chains (n):

$$M_n = \frac{\sum_{i=1}^{n} M_i n_i}{\sum_{i=1}^{n} n_i}$$

where M_i is the molecular weight of the i-th polymer chain in a given sample, n_i is the number of polymer chains of M_i. The weight average molecular weight is given by the total molecular weight divided by their weight fractions:

$$M_w = \frac{\sum_{i=1}^{n} {M_i}^2 n_i}{\sum_{i=1}^{n} M_i n_i} \tag{1.2}$$

Other than using the average molecular weight, polydispersity index (PDI) can also be used to characterize a polymer product. The PDI measures the molecular weight distribution in a given polymer sample:

$$PDI = \frac{M_w}{M_n} \tag{1.3}$$

Due to the nature of how PDI is defined, a PDI value is equal to or greater than 1. A PDI value of greater than 1 indicates that the polymer sample has a wider distribution of molecular weights. A PDI value of 1 indicates that all the chains in the polymer sample has the same molecular weight, and the sample is said to be monodisperse.

For an amorphous material in a liquid state to go to a solid state without being crystallized, a very fast cooling process is required. During the liquid-solid transition, several types of relaxations occur in the amorphous material: α and β relaxations. α relaxation is caused by diffusive motions. Diffusive motions occur when center-of-mass of molecules moves around. Upon fast cooling, the diffusion of the particles slows down until a liquid material becomes solid. A relaxation time, τ for α relaxation follows the Vogel-Fulcher-Tammann (VFT) equation:

$$\tau(T) = \tau_\infty \exp(\frac{DT_0}{T - T_0}) \tag{1.4}$$

where τ_∞ is the extrapolated relaxation time at infinite temperature, T_0 is a fitting parameter of temperature where relaxation time diverges from VFT equation and D is Vogel activation energy. It is noted that τ is used to characterize each relaxation process. On the other hand, β relaxation is a low-temperature relaxation related to 'local mode' motions [12]. Different from diffusive motions, local motions occur when center-of-mass of molecules does not move. The β relaxation time, as a function of temperature follows

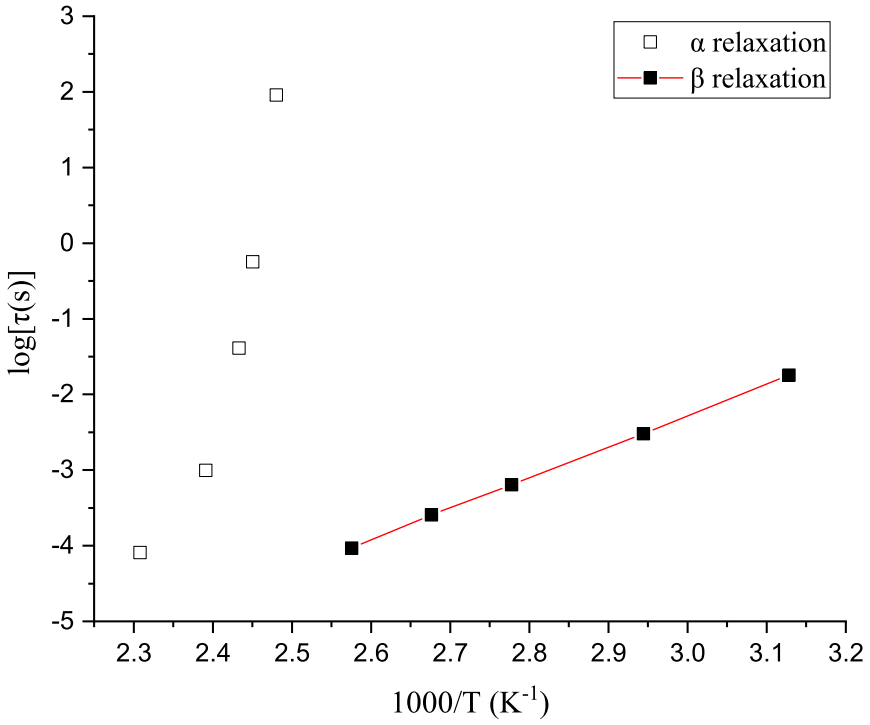

Figure 1.1: Temperature dependence of α and β relaxation times for PMMA by R Casalini et al., Macromolecules, 44(17):6928-6934,2011 [1].

Arrhenius model:

$$\tau(T) = \tau_0 \exp(\frac{\Delta E_a}{k_B T}) \tag{1.5}$$

where ΔE_a is the activation energy, τ_0 is a preexponential factor and k_B is Boltzmann's constant. As shown in Figure 1.1, the Arrhenius law gives a linear relationship between $\log\tau$ and $1/T$. Viscosity is an essential physical property in the study of the structural relaxation process. According to the VFT expression, viscosity is related to temperature through $\eta \propto exp(\frac{DT_0}{T-T_0})$[13].

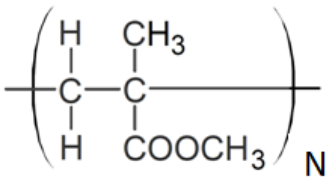

Figure 1.2: Chemical structure of polymethyl methacrylate.

Polymethyl methacrylate (PMMA) is a polymer of methyl methacrylate. The chemical structure of PMMA is shown in Figure 1.2. Its properties such as superior resistance to UV light, high toughness and high chemical resistance hint a promising application in the field of architecture, electronics protection, building construction, etc. [14]. Due to diffusive motions and local motions of polymeric glass (e.g PMMA) chains, α and β relaxation processes of PMMA can be observed in a relaxation experiment. As shown in Figure 1.3, β relaxation peak of PMMA is observed at 50 °C, and α relaxation peak is observed at around 130 °C. Since the curves of both relaxations are symmetric about their peaks, a Gaussian equation can be used to describe the relaxations. It is noted that relative amplitudes of β relaxation to α relaxation strongly depend on a molecular weight [15].

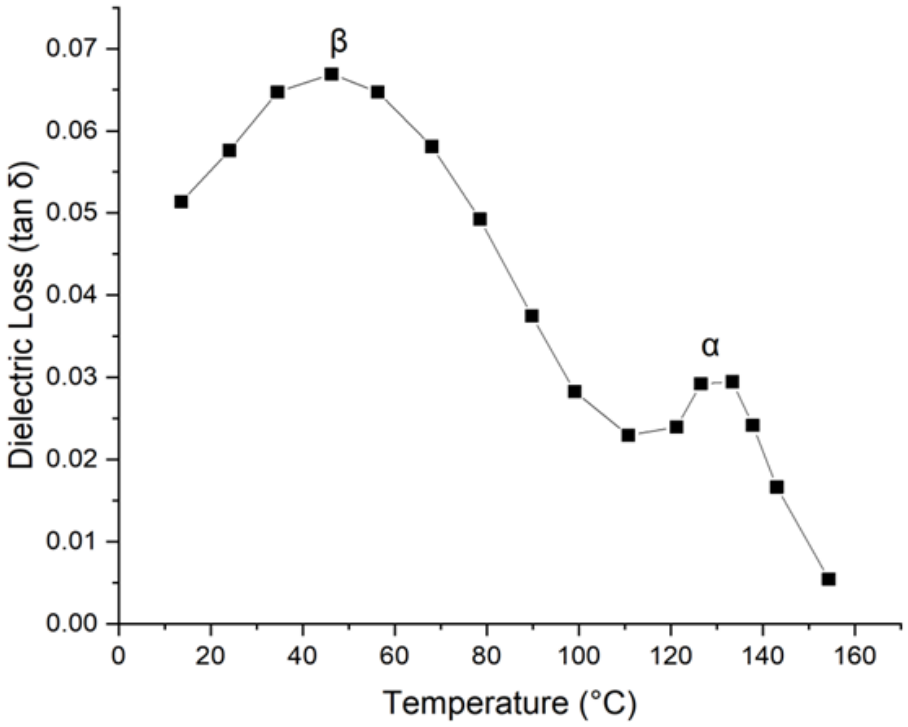

Figure 1.3: Dielectric loss tangent as a function of temperature in PMMA by Williams, G., 1967 [2]

1.2 Glass and Stable Glass

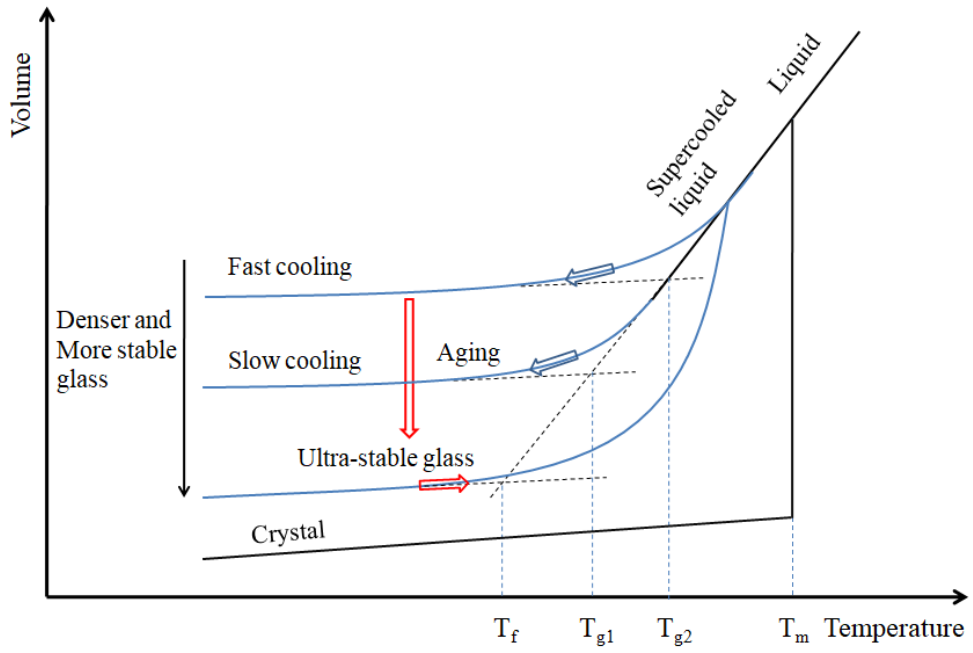

Figure 1.4: Volume as a function of temperature in a glass system.

Figure 1.4 shows volume as a function of temperature in a glass. As shown in the figure, a glass is defined as a non-equilibrium amorphous solid produced by rapidly cooling a liquid [16]. When the liquid is cooled at a constant rate, it can either crystallize at a melting point (T_m) or become a supercooled liquid. The supercooled liquid is in a metastable state. A gradual transition from the metastable supercooled liquid state to the amorphous solid state is termed as glass transition. During the transition process, molecular motions are so slow that the system can no longer stay in an equilibrium state. Relaxation processes occur in the glass transition region. The temperature range where a glass transition occurs is called glass transition temperature (T_g). It is lower than the melting point of the material. Usually, α relaxation can be observed above T_g, while other relaxations occur below T_g.

It is found that a cooling rate has an effect on T_g in the process of forming glasses. Another form of the Vogel-Fulcher-Tammann (VFT) equation can reflect the relationship between the cooling rate and T_g:

$$v = v_0 \exp(\frac{B}{T_g - T_0}) \tag{1.6}$$

where v is the cooling rate, v_0 is a preexponential factor, T_0 is a fitting parameter of temperature where relaxation time diverges from VFT equation, and B is a material-related factor. A more detailed description of the empirical relation is given in Figure 1.4. The upper curve in Figure 1.4 represents a glass with higher T_g prepared at a relatively high cooling rate, while the lower curve represents a glass with a lower T_g prepared at a low cooling rate. After the equilibrium material is quenched to the non-equilibrium glassy state, the obtained glassy material is found to approach equilibrium in volume-relaxation studies of glassy materials [17]. The process of attempting to establish equilibrium is called physical aging. It should be noted that aging process occurs only in non-equilibrium glasses. If physical aging occurs far below T_g, the aging process will last for extremely long. However, upon aging close to T_g, aging will stop at a certain time, which is seen as the glass equilibrium time [18]. Physical aging leads to changes in temperature-dependent properties of glass such as stability, dielectric constant and dielectric loss. The effect of physical aging can be eliminated by heating the glass above T_g. The glass prepared by aging at an extremely low rate has an exceptionally high density and a superior kinetic stability. Such glass is called stable glass.

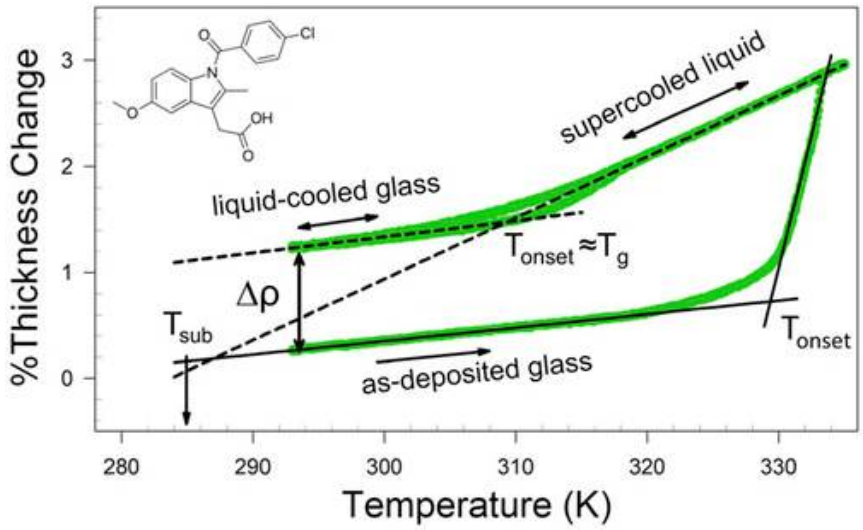

Figure 1.5: Spectroscopic ellipsometry measurements of film thickness for a vapor-deposited stable glass of indomethacin by Ediger, M. D.,The Journal of chemical physics, 147(21), 210901., 2017 [3].

Fictive temperature (T_f) is an essential parameter defined as the intersection of the equilibrium liquid line and the non-equilibrium glass line during heating process. T_f has been employed for characterizing stability and structure of glassy materials. The difference between T_f and T_g is that T_f is only measured during solid-to-liquid transition whereas T_g is usually measured during liquid-to-solid transition. T_f is equal to T_g when a glass has not experienced physical aging or has been cooled down immediately after being heated up (rejuvenation). As shown in Figure 1.4, both T_g and T_f of ordinary glasses can be described as the intersection between the extrapolated glass line and the equilibrium liquid line. Moreover, the ultra-stable glasses, obtained by physical aging, have a lower T_f value compared to the ordinary glasses.

A natural method to obtain such stable glasses is to age ordinary glasses far below T_g for thousands or even millions of years [19]. In this project, physical vapor deposition (PVD) is used to produce stable glasses with the same characteristics as ideal stable glasses

obtained by aging. PVD is an advanced and efficient method utilized to prepare stable glasses similar to the stable glasses obtained by aging [20]. This method can be regarded as a deposition process to produce thin films by condensing a solid/liquid material from a vaporized state onto a substrate. Many different materials (e.g. molecular glasses, metallic glasses) have been made to form stable glasses by using PVD. As shown in Figure 1.5, the indomethacin glasses produced by PVD exhibit characteristics of exceptionally high density, shown by smaller thickness than the ordinary glasses. The kinetic stability of glasses can be reflected by the onset temperature, which is defined by the temperature where a non-equilibrium glassy state turns into a supercooled liquid state. Compared to the ordinary liquid-cooled glass, the onset temperature of the stable as-deposited glass is higher. This phenomenon indicates that it takes longer for the stable glasses to transform into supercooled liquid. Accordingly, the kinetic stability of the stable glasses is greater than that of the ordinary glasses.

In PVD, a glass sample is vapor-deposited onto a substrate at a temperature below T_g. The temperature below T_g allows the glass to have surface mobility and re-orientate configurations towards lower entropy and lower energy [4]. At the temperature below T_g, the top layer of the glass possesses more mobility than the interior of the glass. If the deposition rate is sufficiently low, the molecules at the surface can establish a state close to equilibrium [21, 22]. Then the subsequent layer in the glass can approach an equilibrium state as well. Therefore, a slower deposition rate contributes to yielding stable glasses with greater kinetic stability. An appropriate substrate temperature lower than T_g is considered as another key factor for yielding denser stable glasses. As shown in Figure 1.6, the best substrate temperature to deposit the glass sample of indomethacin is around 0.85 times of its glass transition temperatures (T_g) [23]. A deposition process at a too high temperature results in a fast equilibration process towards a supercooled liquid state and formation of

normal liquid-cooled glasses. If the substrate temperature is too low, surface mobility is so low that the equilibrium process in stable glasses will be restricted.

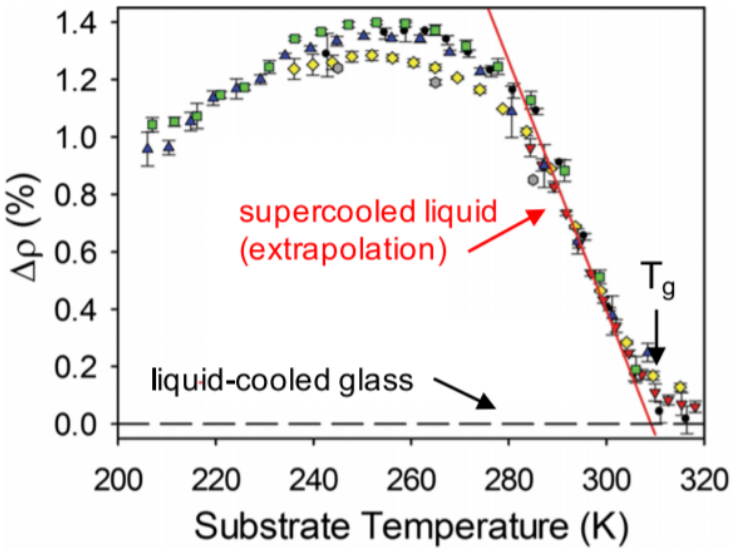

Figure 1.6: The density of vapor-deposited glasses of indomethacin relative to liquid cooled glasses as a function of substrate temperature by Ediger, M. D.,The Journal of chemical physics, 147(21), 210901., 2017 [3].

1.3 β Relaxation in Stable Glass

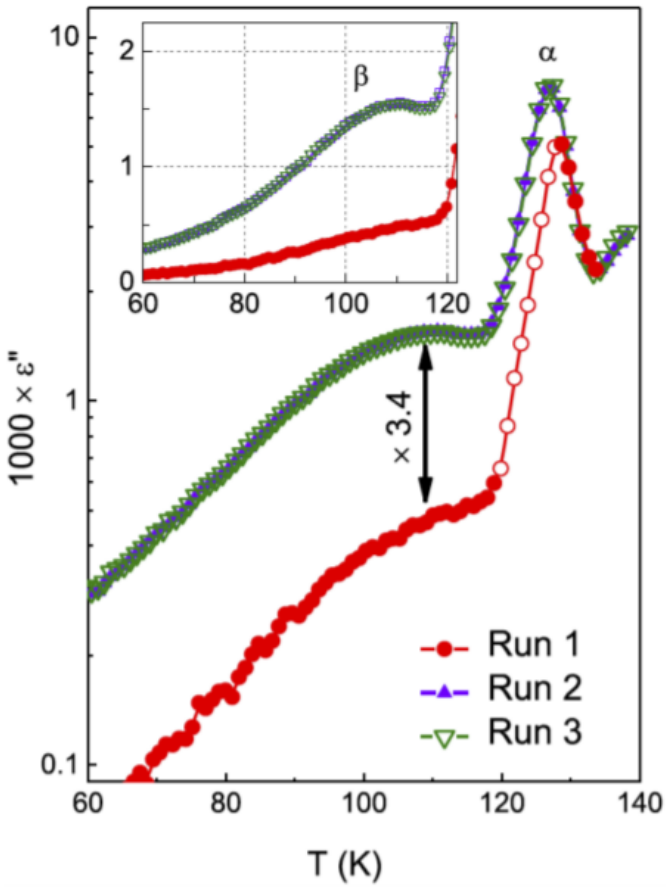

Figure 1.7: Dielectric measurement of a stable glass of toluene (vapor-deposited at 98 K) by Yoon, H., Macromolecules, 50(11), 4562- 4574.,2017 [4].

Due to low entropy in stable glasses [4, 24], local motions have been restricted and molecular packing has become more efficient in the stable glass system. Those changes lead to different β relaxation peaks between stable glasses and ordinary glasses.

In the previous research done by HB Yu et al. [25], the β relaxation peaks of small molecules (toluene) are compared between the stable vapor-deposited glasses and the reju-

venating ordinary glasses transformed from stable glasses. As shown in Figure 1.7, run 1 represents the dielectric loss of the stable glasses while run 2 and 3 represent the dielectric loss of the ordinary glasses. The figure shows that 70% of the β-relaxation amplitude is suppressed at about 110 K in the vapor-deposited stable glasses of toluene. The amplitude of the β relaxation peak is reduced due to the hindered local atomic motions in the stable glasses. The hindered local motions in glassy materials arise from a more efficient molecular packing [26]. The hindered local motions in ultra-stable glasses do not only affect the β relaxation amplitude but also increase β relaxation time in glassy materials.

Furthermore, molecular reorientation in a glass system is restricted to certain cone angles. Among all the angles of the toluene molecules, 90% of them are small cone angles ranging from 2° to 10° whereas the rest 10% are large cone angles ranging from 40° to 50°. The minority of molecules with large cone angles contribute to 50% of relaxation amplitude [27, 28]. Therefore, the suppression of β relaxation in the stable glasses of toluene may arise mainly from vanishing of those large cone angles or decrease in all the cone angles. Those changes in cone angles can lead to a more efficient packing in the glass system.

For the stable glasses of toluene, the suppression of β relaxation can be tuned by adjusting the substrate temperature and the deposition rate [24]. The two factors are related to the stability of the glasses. The most effective temperature for toluene stable glasses ranges between 0.6 and 0.9 T_g, where the suppression extent reaches maximum. The β relaxation amplitude decreases with the reduction in deposition rate when the deposition rate is above 1nm/s. However, below a critical deposition rate of 1nm/s, the suppression of β relaxation amplitude is independent of the deposition rate. Therefore, 1nm/s is the deposition rate to produce the stable glasses of toluene with the greatest kinetic stability.

In this project, it is postulated that β relaxation peak in stable polymeric glasses may also be suppressed in dielectric measurements. Accordingly, the amplitude of β relaxation

in stable polymeric glasses can possibly be changed by adjusting substrate temperatures and deposition rates.

1.4 Outline of Experiment

In this thesis, ordinary glasses and stable glasses of PMMA are the subjects of dielectric relaxation studies. The investigations of PMMA have been focused on aspects of degree of polymerization, polydispersity, glass transition, physical aging and relaxation process. Like other glassy materials, stable glasses of PMMA can be produced by physical vapor deposition of ordinary oligomeric PMMA. Below glass transition temperature, the β relaxation of the stable glasses of PMMA has been measured in dielectric measurements. The suppression of β relaxation in polymeric stable glasses of PMMA may be expected. For the purpose of studying the relaxation of the ordinary and stable glasses of PMMA, we have performed experimental methods including drop-coating, annealing, distillation, physical vapor deposition (PVD), and the measurement of dielectric loss in our research.

In Chapter 2, more detailed experimental procedures for making and measuring PMMA films will be provided. Chapter 3 will give us insights into dielectric measurements on stable glasses of PMMA.

Chapter 2

Experimental Details

2.1 Dielectric Relaxation Basics

The relaxation response of dielectric materials after being aligned by an electric field is called dielectric relaxation [29]. To embark on dielectric relaxation studies, it is useful to first learn relative permittivity. The relative permittivity of the material $\varepsilon_r(\omega)$ is defined as the frequency-dependent permittivity $\varepsilon(\omega)$ divided by the permittivity of vacuum ε_0 (ε_0=8.854×10^{-12}F/m):

$$\varepsilon_r(\omega) = \frac{\varepsilon(\omega)}{\varepsilon_0} \tag{2.1}$$

The relative permittivity measured at infinity high frequencies is ε_∞. ε_∞ is determined by:

$$\frac{\varepsilon_\infty - 1}{\varepsilon_\infty + 2} = \frac{4}{3}\pi \bar{N} \alpha_e \tag{2.2}$$

where $\bar{N}$ is the number of molecules per unit volume, α_e is average polarization per molecule.

ε_s is the static relative permittivity measured at the frequency of zero. It is related to short-range interactions between molecules. It has quantitative relationship with ε_∞, which is given by:

$$\varepsilon_s - \varepsilon_\infty = \frac{3\varepsilon_s}{2\varepsilon_s + \varepsilon_\infty} \frac{4\pi \bar{N}}{3kT} (\frac{\varepsilon_\infty + 2}{3})^2 g\mu_0^2 \tag{2.3}$$

where g is the orientation correlation parameter (approximately equal to 1), μ_0 is the external moment of the molecule when surrounded by vacuum. Based on previous literature [2, 30], the ε_∞ value for bulk PMMA is 3.5 and the quantitative relationship between ε_s and ε_∞ is ε_s /ε_∞ =5. Hence, the ε_s for bulk PMMA is calculated to be 17.5.

For a material which exhibits dielectric relaxation, its relaxation permittivity $\varepsilon_r(\omega)$ is a complex number given by:

$$\varepsilon_r(\omega) = \varepsilon_\infty + (\varepsilon_s - \varepsilon_\infty)/(1 - j\omega\tau) \tag{2.4}$$

where τ represents relaxation time and ω is angular frequency [31].

From equation 2.4, we know that the relative permittivity of a dielectric material is not a real number, it also includes an imaginary part. The real part and the imaginary part can be separated into two terms in the expression of relative permittivity $\varepsilon_r(\omega)$:

$$\varepsilon_r(\omega) = \varepsilon_r^{'} - j\varepsilon_r^{''} \tag{2.5}$$

where $\varepsilon_r^{'}$ is the real part representing storage factor and increasing the capacitance, $\varepsilon_r^{''}$ is the imaginary part representing loss factor [32].

The expressions of the imaginary and the real parts can be given by:

$$\varepsilon_r^{''} = \omega\tau(\varepsilon_s - \varepsilon_\infty)/(1 + \omega^2\tau^2) \tag{2.6}$$

$$\varepsilon_r^{'} = \varepsilon_\infty + (\varepsilon_s - \varepsilon_\infty)/(1 + \omega^2\tau^2) \tag{2.7}$$

where ω=$2\pi f$, f=1000Hz (all the dielectric measurements have conducted at the frequency of 1000Hz), the relaxation time τ is given by the Vogel-Fulcher equation. The parameters ($\log(\tau/\mathrm{s})$ = -10.9 $\pm$ 0.2, $T_0(\mathrm{K})$ = 238$\pm$4, D = 75$\pm$10) in Vogel-Fulcher equation is obtained from the work of Casalini et al [33], where the PMMA sample they used has an average molecule weight of 1040g/mol.

The relative permittivity of a dielectric material in measurements at a constant frequency is given by:

$$\varepsilon_r^{'}(\omega) = \frac{C}{C_0} \tag{2.8}$$

where $\varepsilon_r^{'}(\omega)$ is the real part of $\varepsilon_r(\omega)$, C is capacitance of a capacitor filled with dielectric substance between electrodes, C_0 the capacitance only with a vacuum between electrodes. A capacitor is designed for storing electric charge, and capacitance is a property of a capacitor to indicate the amount of stored charge on capacitor electrodes. $\varepsilon_r^{'}(\omega)$ is only dependent on the substance material between electrodes.

During dielectric measurements, loss tangent tanδ is the measure of the dissipation factor expressed by the ratio of loss factor $\varepsilon^{''}$ to storage factor $\varepsilon^{'}$:

$$tan\delta = \frac{\varepsilon_r^{''}}{\varepsilon_r^{'}} \tag{2.9}$$

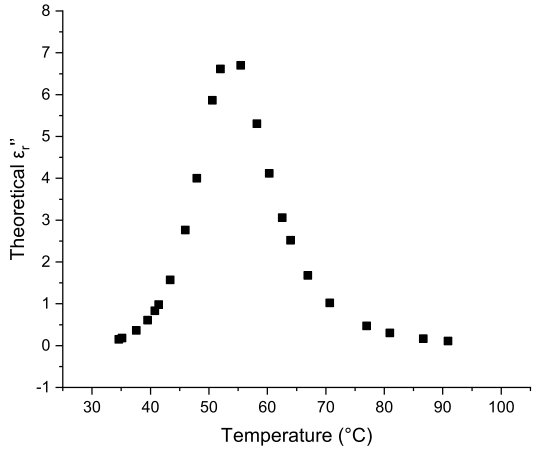

a.

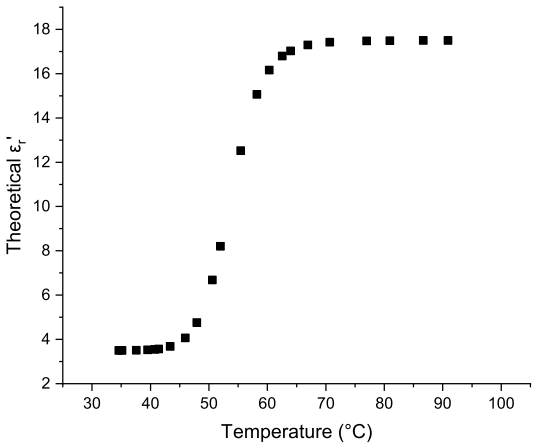

b.

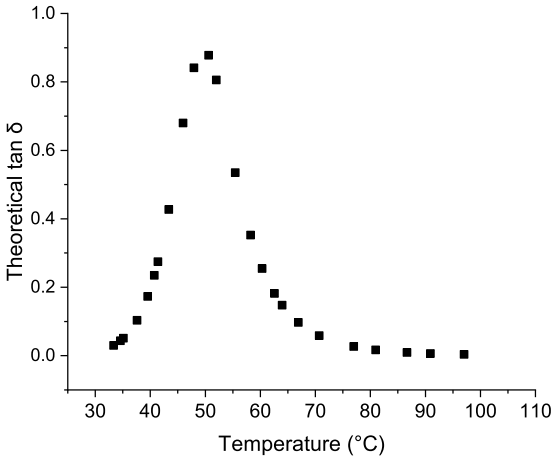

c.

Figure 2.1: Dielectric loss as a function of temperature at 1kHz for vapor-deposited stable glasses of PMMA and corresponding Gaussian fitting curves. (a) $\epsilon_r^{''}$ (b) $\epsilon_r^{'}$ (c) tan δ as a function of temperature for bulk PMMA (N=10).

The diagram of the $\varepsilon_r^{''}$ as a function of temperature for bulk PMMA (Figure 2.1.a) can be generated based on equation 2.6. According to equation 2.7, the curve of the $\varepsilon_r^{'}$ as a function of temperature for bulk PMMA can be generated in Figure 2.1.b. Since storage factor of a capacitor is determined by its capacitance, the curve of storage factor $\varepsilon_r^{'}$ in Figure 2.1.b reflects how capacitance for PMMA changes with temperature. By combining equation 2.6, 2.7 and 2.9, the relationship between $tan\delta$ and relaxation time is described as:

$$tan\delta = \frac{(\varepsilon_s - \varepsilon_\infty)\omega\tau}{\varepsilon_\infty\omega^2\tau^2 + \varepsilon_s} \tag{2.10}$$

By applying all the above equations, $tan\delta$ values at different temperatures can be obtained. The calculation process is used to generate an expected tanδ curve as a function of temperature (Figure 2.1). For this bulk PMMA, the theoretical α relaxation peak is at around 53 °C. It is worth noting that β relaxation does not emerge in the diagrams of Figure 2.1 because VFT equation is only for α relaxation. In Figure 2.1.b, a step starts to show up at 60 °C, which is close to the temperature of the α relaxation peak in Figure 2.1.c.

2.2 Experimental Details

The measurements of dielectric relaxation in polymers were performed by using a capacitor filled with polymethyl methacrylate (PMMA) films. As shown in Figure 2.2.a, the capacitor electrodes were designed to be two 5-mm-thick, 1.9-cm-diameter stainless steel disks. To ensure the disk surface is flat enough, four different aluminum oxide slurries with particle sizes ranging from 5 to 0.05 μm (Mark V Laboratories) were utilized to polish the two metal disks in a fume hood until the surfaces of the disks turned shiny and light silver. Then the disks were rinsed with water and acetone so that the slurry particles could be removed.

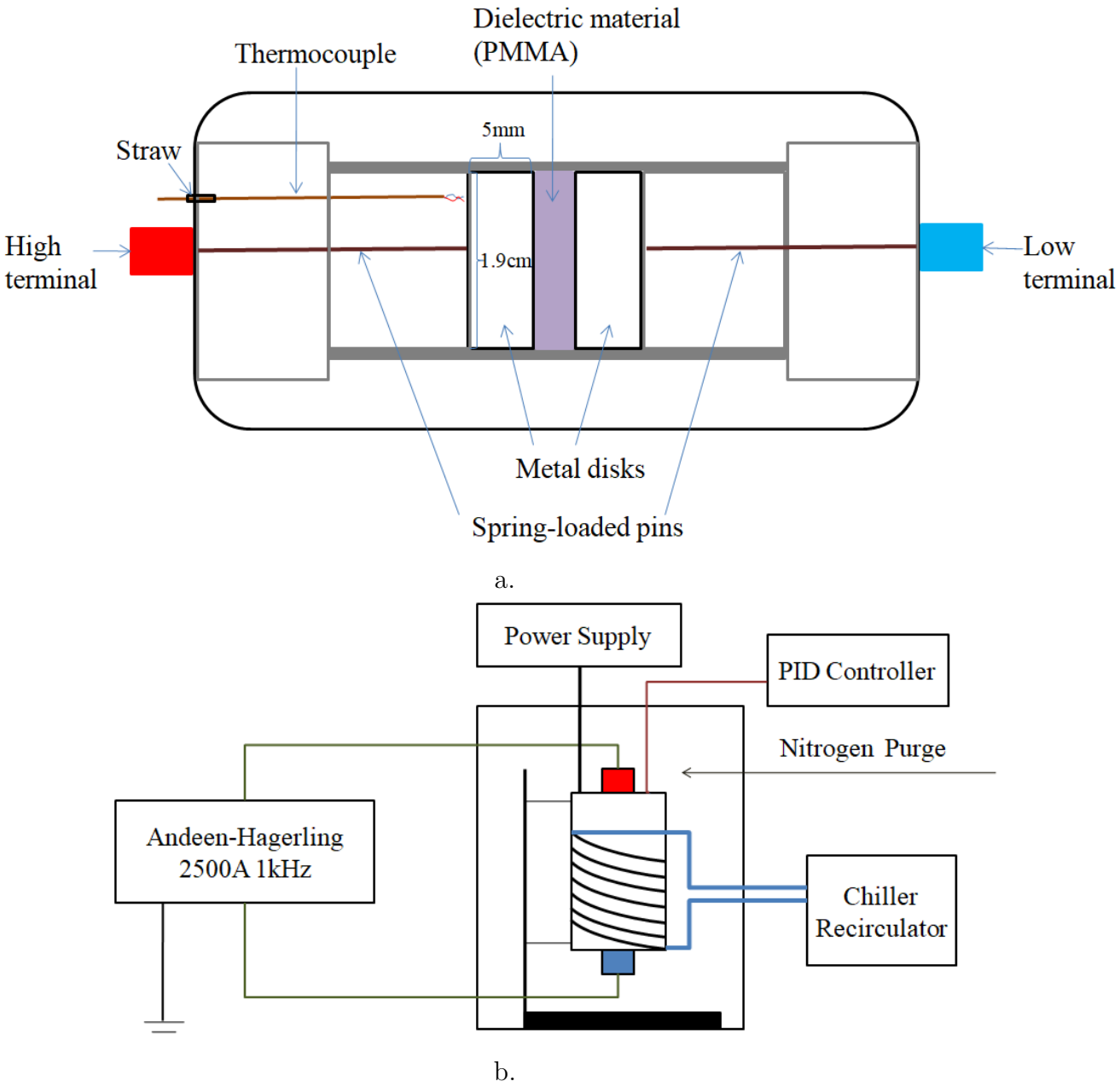

Figure 2.2: Schematic illustration of (a) the capacitor chamber (b) the entire system.

The PMMA sample (M_n=1850g/mol, PDI=1.15, T_g=70℃) used in the dielectric measurement has a syndiotactic content $>$ 85% structure. Each PMMA film was prepared by dropcasting the PMMA sample (in toluene) onto the polished side of one metal disk. The PMMA film coated onto metal disk was annealed overnight at 90℃ so that toluene could be removed from the PMMA films. Then the PMMA-coated metal disk along with a clean disk was put into a chamber for dielectric measurements. The clean disk acted as a reference plate for temperature measurement. A T-type thermocouple was inserted into the capacitor chamber through a hole and utilized to measure the temperature of one of the metal disks. The thermocouple was set through a straw which stuck right in the hole. The straw held the thermocouple in place so that the tip of the thermocouple could be very close to one metal disk but never contacted the disk surface. The other end of the thermocouple was connected to a MICROMEGA PID temperature controller (Model CN77353-C2). The PID controller was used for monitoring temperature changes of the reference disk. The chamber cell was placed in a sealed plastic bag. A nitrogen purge, giving a regulated gas pressure of 0.8 psi, was fixed through the plastic bag to flush the chamber before and during the experiment. The gentle nitrogen flushing can remove atmospheric water vapor in the capacitor chamber and decrease the noise brought by the background.

In this experiment, we used the toluene solutions with different PMMA weight percentage of 3.6% and 0.8% to make dropcoated PMMA films. The dropcoated PMMA films were used as dielectric materials of capacitors. No spacer is used in a capacitor fully filled with the PMMA film made by 3.6% solution. However, four pieces of 3×3-mm^2, 5-μm-thick polytetrafluoroethylene (PTFE) spacers (from Goodfellow) were cut from a large sheet and then used to space one of the electrodes and the dropcoated PMMA film made by 0.8% solution.

The PTFE spacers between capacitor electrodes may have an effect on the dielectric

measurements. Therefore, a plate capacitor only filled with spacers needed to be tested by dielectric measurements. Two cleaned metal disks were prepared as capacitor electrodes. Four pieces of 3×3-mm^2, 5-μm-thick PTFE spacers were used to space the two electrodes. This capacitor partially filled with PTFE spacers was regarded as the background.

All the dielectric measurements were performed by connecting the chamber cell to Andeen Hagerling 2500A 1kHz ultra-precision capacitance bridge. The instrument can be set to measure capacitance C in the unit of pF and dielectric loss tangent $tan\delta$ as a function of temperature. AH 2500A has high sensitivity, low noise and high accuracy. It can collect a precision of 10^{-6} pF for the capacitance and 10^{-8} for the dielectric loss tangent.

The schematic illustration of the entire setup is shown in Figure 2.2.b. AH 2500A was set to be continuous mode to run the measurements. All the cables needed to be disconnected before completing the setting of AH 2500A. After assembling the chamber cell, we pressed the recirculation button and then the chiller button in a VWR® Recirculating Chiller. The recirculation was on to ensure that external noise could be minimized. The chiller kept the recirculating water at 5 °C to control the ramping rate. Then we turned on a Power Supply (Delta Elektonika ES 075-2, output impedance $<$ 250 mOhm) with a constant voltage of 60V to heat the capacitor up to 90 °C.

Afterwards, the power supply was turned off, and the chamber was cooled by the chiller. The temperature scan needed to be done between 25 °C and 90 °C for two cycles to ensure reproducibility of results. During the measurement, the dielectric loss tangent and capacitance of the capacitor were collected and recorded manually every 8 seconds. In the subsequent analysis phase, we took the average of every three adjacent points in the collected data.

2.3 Testing using dropcoated PMMA films

Figure 2.3 shows a illustration of the geometry model for a capacitor fully filled with a thick PMMA film. 3.6% PMMA in toluene was used for dropcasting a relatively thick film on one metal disk. After the coated disk has been annealed and cooled down, another disk was gently placed onto the top of the PMMA film. A capacitor filled with one single PMMA film has been created in this way. The radius of a disk is 0.95 cm. Since the disk is fully covered by PMMA, the radius of the PMMA film is also 0.95 cm. The thickness of the PMMA film can be calculated as below.

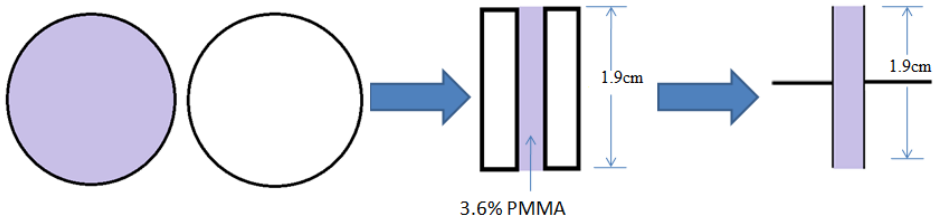

Figure 2.3: An illustration of the geometry model for the capacitor filled with a thick PMMA film.

One drop of the toluene solution was weighed in a Petri dish placed on the scale after pressing TARE. This procedure was repeated for three times. The weights of one drop were measured to be 0.0148g, 0.0131g and 0.0126g. The average drop weight was 0.0135g. Ten drops were used for dropcasting a thick PMMA film in total. Therefore, the total mass of the solution we used is $m_{solution}$ =0.135 g. Since the density of toluene $\rho_{toluene}$ = 0.867 g/cm^3, the PMMA weight percentage wt% is 3.6%, the PMMA mass is given by $m_{solution}$= wt% $m_{solution}$ $\rho_{toluene}$ =0.135g×0.867 g/cm^3×0.036 =4.214×10^{-3}g=4.214×10^{-6}kg. The mass of the PMMA film can be expressed by m_{PMMA}= V_{PMMA} ρ_{PMMA}, where ρ_{PMMA}=1180 kg/m^3, V_{PMMA}=$d_{PMMA}\pi r^2$, the thickness of coated PMMA film at room temperature can

be obtained by:

$$d_{PMMA,RT} = \frac{m_{PMMA}}{\pi r^2 \times \rho_{PMMA}} \tag{2.11}$$

where ρ_{PMMA}= 1180 kg/m^3, m_{PMMA}=4.214mg, r=0.0095m. Therefore, the calculated thickness of PMMA film is 12.6 µm. Since PMMA film will be expanding when it is heated up, the increased thickness of PMMA film is given by:

$$\Delta d_{PMMA} = \alpha_{L,PMMA} \times \Delta T \times d_{PMMA,RT} \tag{2.12}$$

where ΔT represents the increased temperature, $\alpha_{L,PMMA}$ is thermal expansion coefficient, and its value for PMMA is $\alpha_{L,PMMA} = 8{\times}10^{-5}$ K^{-1}.

The measured dielectric loss tangent for this dropcoated 12.6 μm PMMA film is shown in Figure 2.4 as a function of temperature for the capacitor filled with only thick PMMA films. In this figure, only one asymmetrical peak is shown on the dielectric loss curve. Since relaxation peaks should be symmetric, this single peak is formed by adding α and β relaxation peaks together [15]. In Figure 1.3, dielectric loss of both α and β relaxations follow an arbitrary equation which shows a symmetric curve. Therefore, the Gaussian equation ($y = y_1 + \frac{A}{\sqrt{\pi/2}} e^{-2\frac{(x-x_C)^2}{w^2}}$) can be used to describe dielectric loss curve of each relaxation. Accordingly, two different Gaussian function terms were summed up to fit the add-up of α and β relaxation peaks on the measured dielectric loss curve in Figure 2.4. By fitting and analyzing the Gaussian curves, it is found out that α relaxation peaks is at around 62°C while β relaxation peaks is around 48°C. All the values of parameters in equation 2.11 have been shown in Table 2.1.

$$tan\delta = tan\delta_0 + \frac{A_\alpha}{\sqrt{\pi/2}} e^{-2\frac{(T-T_{C,\alpha})^2}{w_\alpha^2}} + \frac{A_\beta}{\sqrt{\pi/2}} e^{-2\frac{(T-T_{C,\beta})^2}{w_\beta^2}} \tag{2.13}$$

where $tan\delta_0$ is offset (the sum-up of the lowest $tan\delta$ values for α and β relaxations), A represents the amplitude of one relaxation peak, w represents the width, T_c represents the temperature of relaxation peak.

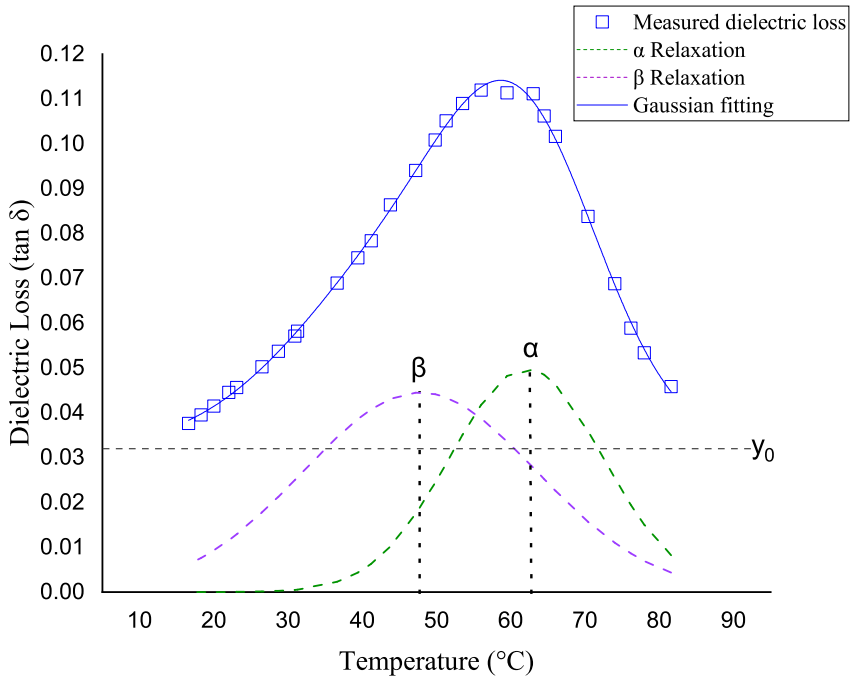

Figure 2.4: Dielectric loss as a function of temperature for a dropcoated thick PMMA film (12.6 μm thick).

Figure 2.5 shows the capacitance curve for the capacitor filled with the 12.6-μm-thick PMMA film. The relative permittivity of the PMMA can be calculated through the measured capacitance. The calculation procedures are shown below.

The equation for capacitance can be described as:

$$C_{PMMA} = \frac{\varepsilon_0 \varepsilon_r^{'} \pi r^2}{d_{RT,PMMA} + \Delta d_{PMMA}} \tag{2.14}$$

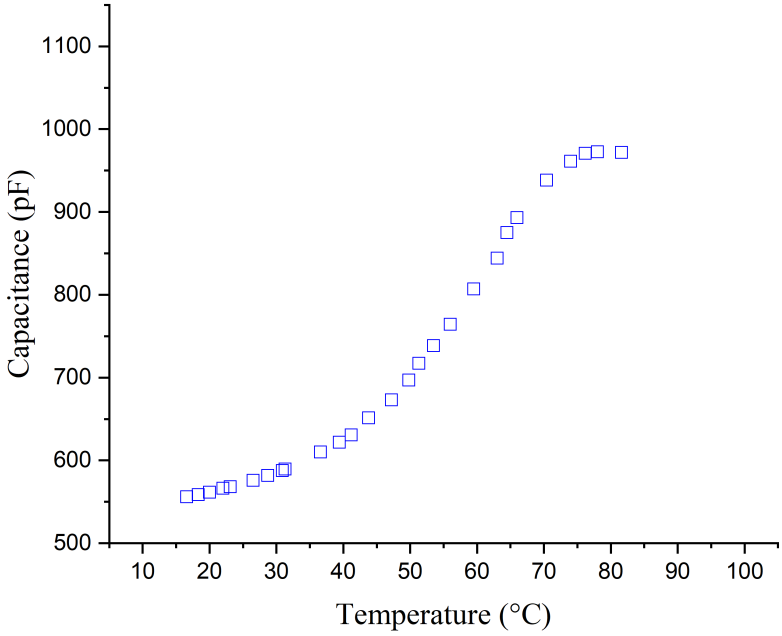

Figure 2.5: Capacitance as a function of temperature for a capacitor fully filled with a dropcoated thick PMMA film (12.6 μm thick).

Table 2.1: The results of the fitting to equation 2.13 for dropcoating the thick PMMA film without PTFE spacers

offset	$tan\delta_0$	$3.2\times10^{-2}\pm3.8\times10^{-3}$
center of α relaxation	$T_{c,\alpha}$	62.1±0.4
width of α relaxation	w_α	20.6±3.2
amplitude of α relaxation	A_α	$6.2\times10^{-2}\pm4.3\times10^{-2}$
center of β relaxation	$T_{c,\beta}$	47.8±9.6
width of β relaxation	w_β	31.4±9.4
amplitude of β relaxation	A_β	$5.6\times10^{-2}\pm2.8\times10^{-2}$

Hence, the relative permittivity of the PMMA at 1kHz can be expressed by:

$$\varepsilon_r^{'}(1kHz) = \frac{C_{PMMA}(d_{RT,PMMA} + \Delta d_{PMMA})}{\varepsilon_0 \pi r^2} \tag{2.15}$$

where permittivity of vacuum is ε_0=8.854×10^{-12}F/m, $d_{RT,PMMA}$ is the thickness of the PMMA film at room temperature. Therefore, the values for relative permittivity at different temperatures can be calculated. Figure 2.6 shows the calculated relative permittivity of PMMA at different temperatures.

Figure 2.7 shows the illustration of a capacitor which is partially filled with a thin PMMA film. 0.8% PMMA in toluene was used to dropcoat a thin film on one metal disk. Four pieces of Teflon spacers were used for separating the disk fully covered with a thin PMMA film and the other clean disk. A capacitor partially filled with one thin PMMA film has been made in this way. In this case, the capacitor can be regarded as two capacitors connected in series, where one capacitor is fully filled with PMMA while the other is only with air. The plate separation of the air capacitor has the same value as the thickness of the PTFE spacer. In this scenario, the mass of each drop can be considered as the same for PMMA solutions with different weight percentage because the two solutions have almost the same viscosity and density. The PMMA mass is given by $m_{solution}$= wt% $m_{solution}$

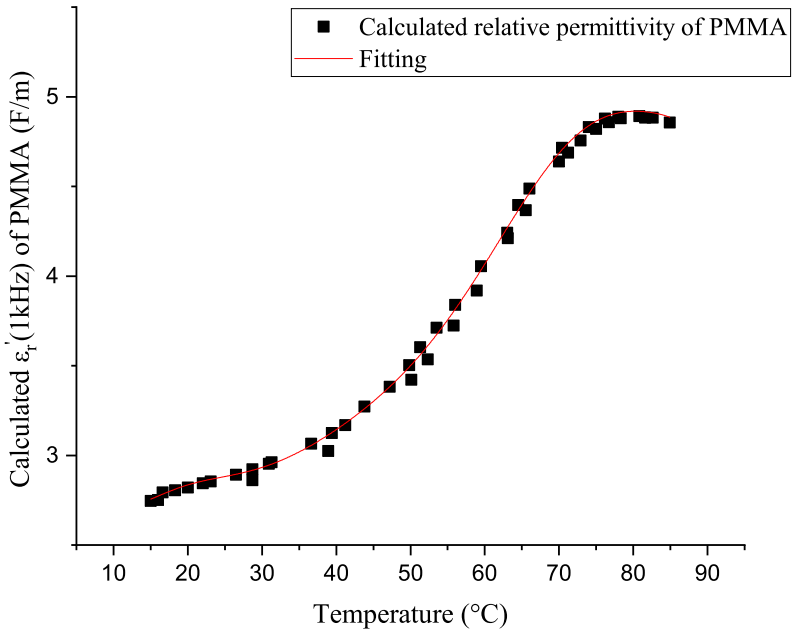

Figure 2.6: Calculated relative permittivity of PMMA as a function of temperature.

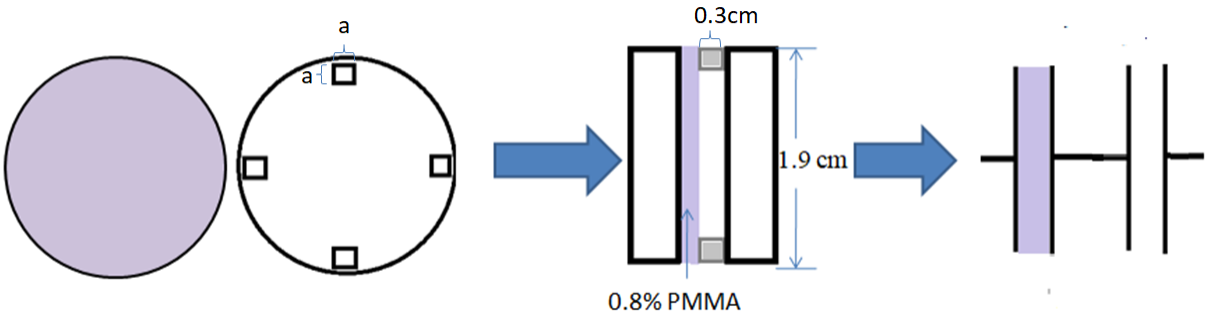

Figure 2.7: An illustration of the geometry model for the capacitor filled with a thin PMMA film and spacers.

$\rho_{toluene}$ =0.135g×0.867 g/cm^3×0.008 =0.95×10^{-3}g=0.95*10^{-6}kg. the thickness of coated thick PMMA film at room temperature can be obtained by equation 2.12. The thickness of PMMA film is calculated to be 2.9 µm. The capacitance for the part filled with PMMA can be obtained by equation 2.14. The capacitance of the part only with air is determined by:

$$C_{air} = \frac{\varepsilon_0 \pi r^2}{d_{PTFE,RT} + \Delta d_{PTFE}} \tag{2.16}$$

where $d_{PTFE,RT}$ is the thickness of PTFE at room temperature, $\Delta d_{PTFE} = \alpha_{L,PTFE} \times \Delta T \times d_{PTFE,RT}$, $d_{PTFE,RT}$=5μm, $\alpha_{L,PTFE}$ = 12x10^{-5} K^{-1}. The capacitance of the PTFE spacers are negligible here. Hence, the capacitor filled with one thin dropcoated PMMA film can be regarded as the air capacitor and the PMMA capacitor connected in series. Therefore, the total capacitance for this model is expressed by:

$$C_{total} = \frac{1}{\frac{1}{C_{PMMA}} + \frac{1}{C_{air}}} \tag{2.17}$$

By using the relative permittivity $\varepsilon_r^{'}$ values from Figure 2.6, the theoretical capacitance for the PMMA part can be calculated. It should be noted that the calculation model is based on the geometry of perfectly-smooth capacitor plates. However, the actual capacitor is not made by two perfectly smooth plates.

As shown in Figure 2.8, the calculated total capacitance is compared with measured capacitance for the capacitor partially filled with a dropcooated 2.9-μm-thick PMMA film. The calculated capacitance values have increased by 6% as the temperature changes from low to high. However, the measured capacitance values have increased by 19% as the temperature changes. The reason for that deviation might be the the nonparallel capacitor plates, which we have mentioned in last paragraph. Detailed explanation will be given in the last section of this thesis.

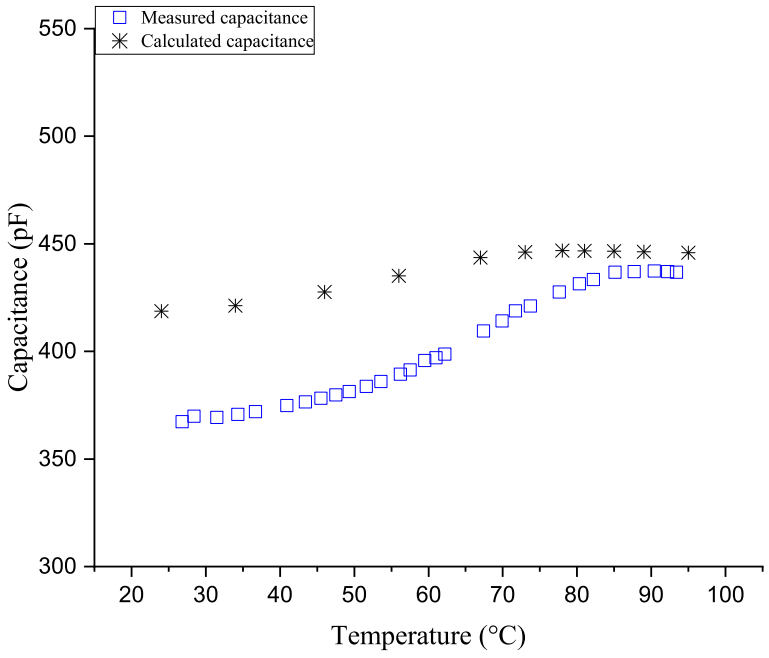

Figure 2.8: Comparison between measured capacitance and calculated capacitance as a function of temperature for a capacitor filled with a thin dropcoated PMMA film (2.9 μm thick) and PTFE spacers (5 μm thick).

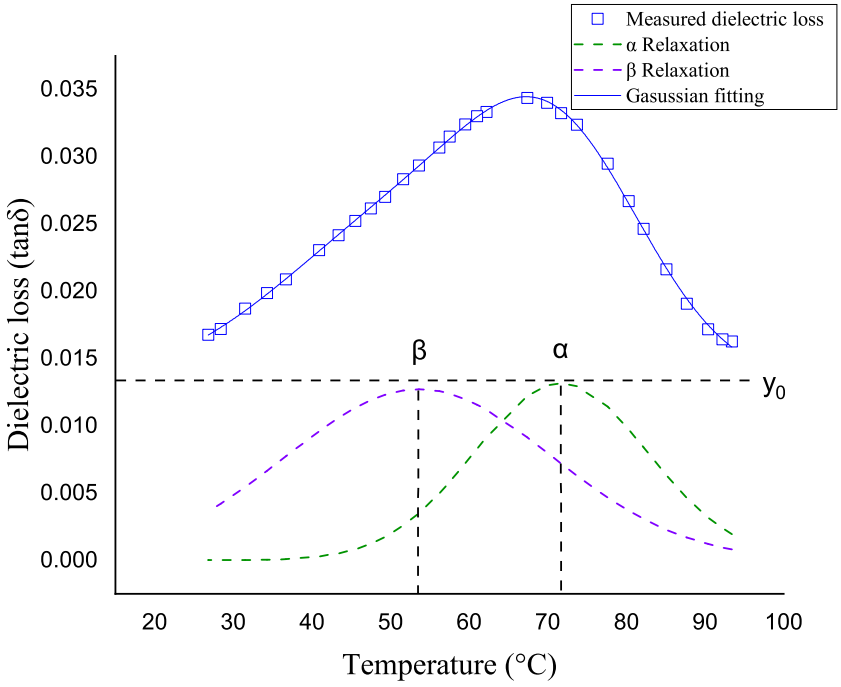

Figure 2.9: Dielectric loss as a function of temperature for a dropcoated thin PMMA film (2.9 μm thick).

Figure 2.9 shows the dielectric loss tangent varying with temperature for the dropcoated 2.9 μm PMMA film. In this figure, the data of background (capacitor filled only with PTFE spacers) has been subtracted from the original data of the measured dielectric loss. Therefore, Figure 2.9 shows the dielectric loss as a function of temperature for only a dropcoated PMMA film. The dielectric loss $tan\delta$ of the background part as a function of temperature is shown in Figure 2.10. An exponential fitting equation ($y = y_0 + A_1 exp(T/b)$) can be used to describe the background. The variables in this term are given by: y_0=$7.3\times10^{-5}\pm1.8\times10^{-6}$, A_1=$8.8\times10^{-8}\pm2.1\times10^{-8}$, b=10.6 ± 0.3.

Similar to Figure 2.4, α and β relaxations merge together on the dielectric curve in Figure 2.9. By fitting the sum-up of two Gaussian function terms based on the measured dielectric loss curve, we can also figure out the location of α and β relaxation peaks in this setting. All the parameters have been summarized in Table 2.2. α relaxation peak is at 72°C and β relaxation peak is at 54°C. The shapes of α and β relaxation peaks in Figure 2.9 are similar to those in Figure 2.4. This proves that the dielectric materials used for the dielectric measurements are from the same PMMA sample.

Furthermore, for either the thin PMMA film or the thick PMMA film, the step on the capacitance curve emerges at the temperature which is slightly higher (around 7 °C higher) than the temperature of the α relaxation peak. Accordingly, it can be deduced that, in the dielectric measurements of the same dielectric material, the steps on the capacitance curve are highly related to the relaxation peak.

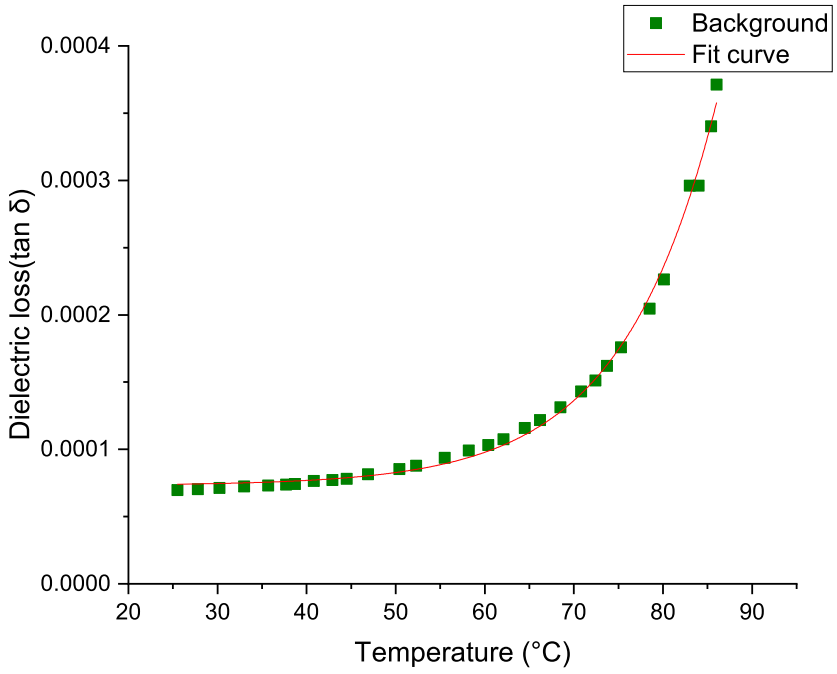

Figure 2.10: Dielectric loss as a function of temperature for the background setting.

Table 2.2: The results of the fitting to Equation 2.13 for dropcoating the thin PMMA film with PTFE spacers

offset	$tan\delta_0$	$1.3\times10^{-2}\pm7.7\times10^{-4}$
center of α relaxation	$T_{c,\alpha}$	71.7±0.8
width of α relaxation	w_α	22.2±2.5
amplitude of α relaxation	A_α	$1.7\times10^{-2}\pm8.9\times10^{-3}$
center of β relaxation	$T_{c,\beta}$	53.6±7.7
width of β relaxation	w_β	33.9±8.2
amplitude of β relaxation	A_β	$1.6\times10^{-2}\pm5.0\times10^{-3}$

Chapter 3

Dielectric Relaxation Measurements on PMMA Glass Produced by Vapor Deposition

3.1 Techniques for Producing Stable Glass films

Physical vapor deposition (PVD) is a standard technology for fabricating and stacking organic thin films. As mentioned in Section 1.1, none of the current polymerization methods can yield monodisperse polymers. Therefore, vacuum distillation prior to the deposition process has been developed to purify polydisperse polymer samples and obtain monodisperse fractions [34]. Physical vapor deposition and distillation are two technologies that will be introduced in this section.

PVD plays an essential role in producing thin films of both inorganic and organic molecules. There are several methods to achieve the production of thin films via PVD. As

shown in Figure 3.1, direct evaporation is carried out by using a polymer as the source material for evaporation. Direct evaporation is the conventional vapor deposition where no chemical bonds were formed at the film/substrate interface [35]. During the process, the vapor-deposited films are physically adsorbed on the substrate surface. This method can produce deposited films on any type of substrate material regardless of the chemical properties of the substrate [36, 37]. Therefore, direct evaporation is a favorable method for producing stable glass of thin polymer films on metal disks in our research project.

The fractional distillation process prior to PVD can effectively produce purified monodisperse polymers. Compounds with different molecular weights can be separated via fractional distillation. The technology is performed based on the difference in vapor pressures of different compounds. Usually, the distillation process occurs in a vacuum chamber. Small compounds with high vapor pressure are evaporated first and large components with low vapor pressure are evaporated later. Ultimately molecules with different sizes are separated, and monodisperse samples can be obtained. It should be noted that vacuum distillation is mainly applied in short polymer chains rather than long polymer chains samples to avoid thermal degradation. Short polymer chains can go through vacuum distillation without thermal degradation. However, long polymer chains require a much higher temperature to evaporate due to their low vapor pressure. The high temperature may cause breaking of covalent bonds and thermal degradation.

PVD can be applied in the production of many types of stable polymeric glass such as polystyrene. Figure 3.2 shows the molecular weight distribution of polystyrene source materials and deposited films. The average N value of the source material is 10.4. As shown in Figure 3.2, the molecular weight distribution of polystyrene source material becomes narrow after vapor deposition, suggesting that PVD can produce highly purified monodisperse polymer fractions [5, 38]. The highly monodisperse samples obtained via

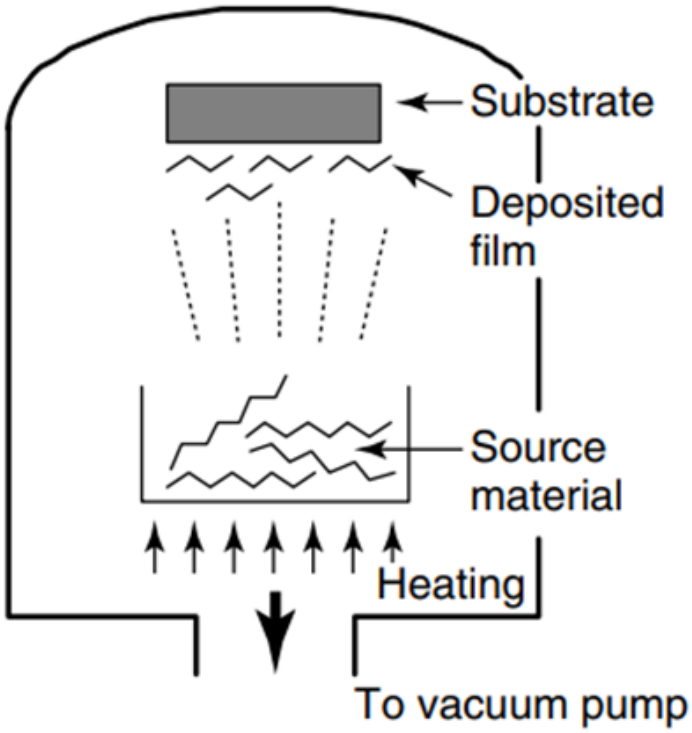

Figure 3.1: Direct evaporation for physical vapor deposition of polymer thin films by Usui, H., Preparation of polymer thin films by physical vapor deposition,2011 [5].

deposition has the degree of polymerization (N) value dependent on the temperature of its source material [6, 39]. As the temperature of the source material increases, the average N of the vapor-deposited films increases as well. However, the N value of the monodisperse sample produced from the same source material is restricted. As shown in Figure 3.2, the used polystyrene sample can only produce a vapor-depsoited film with an N value up to 12.2.

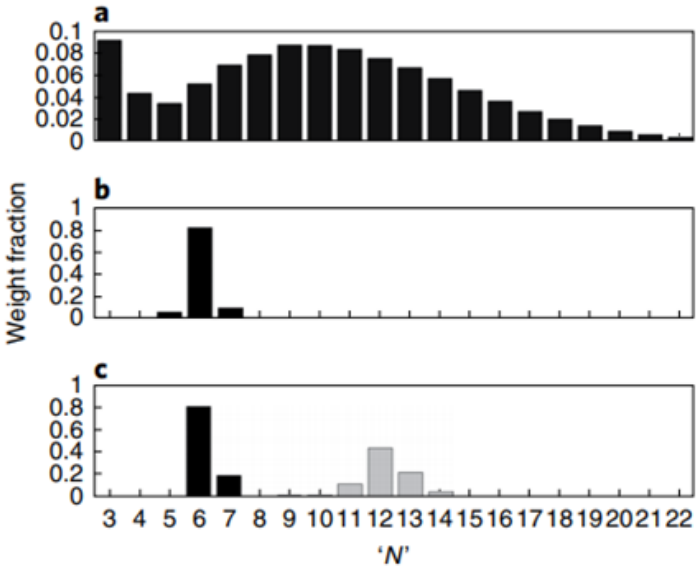

Figure 3.2: Molecular weight distribution of as-purchased polystyrene sample and vapor deposited polystyrene sample at different source temperatures. a. source material, b. after distillation, c. after deposition. by Adam Raegen et al.,Ultrastable monodisperse polymer glass formed by physical vapour deposition, Nature Materials, 19(10), 1110-1113,2020 [6].

3.2 Experimental Details

The PMMA samples used for PVD and dielectric measurement have a molecular weight of 1000g/mol and a PDI value of 1.3 (T_g is measured to be around 50°C by DSC). Since current polymerization methods cannot yield synthesized monodisperse polymers, fractional

distillation was developed for purifying polymers and obtaining monodisperse polymers. In the next step, the distilled polymer sample was vapor-deposited onto a substrate at the temperature of 5°C. The deposition of PMMA was performed by using ORCA organic evaporation mounted on a thin film deposition system-Korvus technologies HEX deposition system. The precise control of low-temperature evaporation in ORCA organic deposition source is achieved by cooling a highly thermal conductive crucible inside the deposition system. The sample was cooled by a Peltier cooler to reach the substrate temperature of 5°C. Deposition rate, as indicated by a quartz-crystal monitor (QCM), was set to be 0.02 nm/s in this deposition process. Ultimately, two PMMA stable films were vapor-deposited on two metal disks, and four pieces of PTFE spacers were placed onto the periphery part of either one of the disks. The following procedures for the dielectric measurement of stable glass were the same as that of ordinary glass in section 2.2. Since the average molecular weight of the produced vapor-deposited PMMA glass was quite small, the temperature range for running multiple cycles was from 20 to 75°C.

3.3 Dielectric Relaxation of PMMA Stable Glass

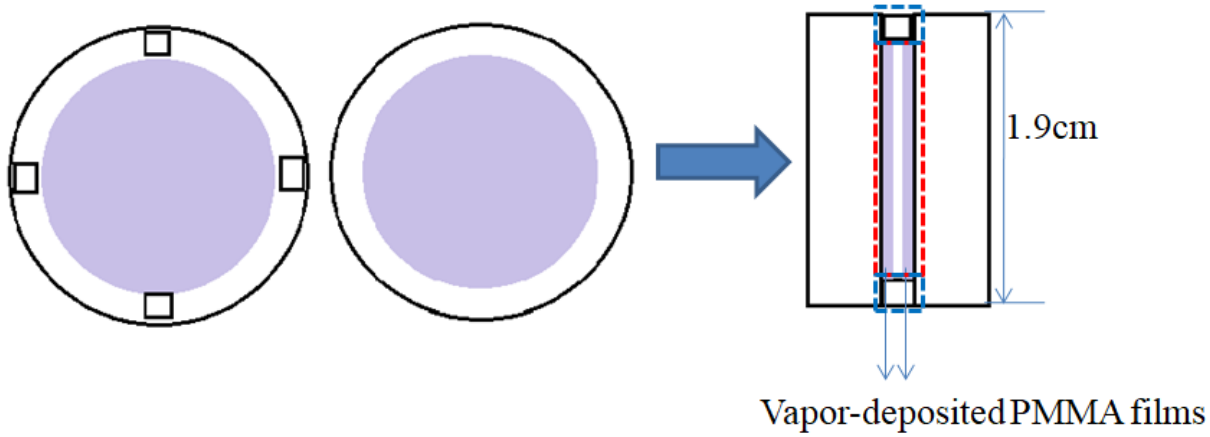

Figure 3.3: An illustration of the geometry model for the capacitor filled with two vapor-deposited PMMA films separated by spacers.

Figure 3.3 shows the illustration of geometry for a capacitor: front view(left), side view(right). As shown in the figure, four pieces of 3mm×3mm PTFE spacers separate two electrodes as well as vapor-deposited PMMA films, indicated by purple regions. This capacitor is composed of two parts: the center part is partially filled with PMMA films (marked with red dashed lines), the outer part is a ring on the edge of electrodes (marked with blue dashed lines). There is no PMMA in the ring part on the edge. It is assumed that the PTFE spacers in the ring part are ignored in the capacitance calculations. This assumption makes only a small difference because the ring part is mostly occupied by air. The capacitance calculations for the PMMA part and for the ring part on the edge are given as below.

The capacitance of a capacitor, which is partially filled with two PMMA films, can be

expressed by:

$$\begin{aligned} C_{PMMA} &= \frac{1}{\frac{1}{C_{air}} + \frac{1}{C_{PMMA}} + \frac{1}{C_{PMMA}}} \\ &= \frac{1}{\frac{H-t}{\varepsilon_0 S} + \frac{t}{\varepsilon_0 \varepsilon_r' S} + \frac{t}{\varepsilon_0 \varepsilon_r' S}} \\ &= \frac{\varepsilon_0 S}{H} \frac{1}{1 - 2t/H(1 - 1/\varepsilon_r')} \end{aligned} \tag{3.1}$$

where S is the surface area of PMMA film, $S = \pi r_{PMMA}^2$, r_{PMMA}=0.65cm, H is the spacing between two plates, $H = d_{PTFE,RT} + \Delta d_{PTFE}$, the thickness of PTFE at room temperature $d_{PTFE,RT}$ is 5μm, $\alpha_{L,PTFE} \times \Delta T \times d_{PTFE,RT}$, $\alpha_{L,PTFE}$ = 12x10^{-5} K^{-1}. t is the film thickness, $t = d_{PMMA,RT} + \Delta d_{PMMA}$, the thickness of PMMA at room temperature $d_{PMMA,RT}$ is 360nm, $d_{PMMA} = \alpha_{L,PMMA} \times \Delta T \times d_{PMMA,RT}$, $\alpha_{L,PMMA} = 8 \times 10^{-5}$ K^{-1}.

Since the PTFE spacers are negligible, the ring part on the edge can be seen as a capacitor only filled with air. The capacitance of the ring part is given by:

$$C_{ring} = \frac{\varepsilon_0 S_{ring}}{H} \tag{3.2}$$

where $S_{ring} = \pi r^2 - \pi r_{PMMA}^2$, r=0.95cm, r_{PMMA}=0.65cm.

The total capacitance of this capacitor geometry in Figure 3.3 is given by:

$$C_{total} = C_{PMMA} + C_{ring} \tag{3.3}$$

Based on the above calculations for a plate capacitor, the curve for the total capacitance as a function of temperature is generated in Figure 3.4. Figure 3.4 also shows the measured capacitance as a function of temperature for the capacitor filled with two vapor-deposited PMMA films. In this figure, the first heating curve represents PMMA vapor-deposited glasses, while the second heating curve represents PMMA rejuvenated glasses which have

been obtained by heating and cooling the PMMA vapor-deposited glasses. Vapor-deposited PMMA produced by the same method and the same procedures has been proved to exhibit lower T_f and higher density than the rejuvenated glasses [6]. Therefore, the vapor-deposited PMMA glasses we used in this project can be regarded as stable glass. The rejuvenated glasses can be considered as ordinary glasses which have not experienced physical aging. As shown in the 3.4, the calculated results deviate from the measured capacitance curves. This huge deviation may result from the plate capacitor with roughness. Moreover, it can be observed that the minimal capacitance value on the first heating curve is higher than that on the second heating curve. However, the maximal capacitance value on the first heating curve is lower than that on the second heating curve. This is because the density of the stable glasses is smaller than that of the ordinary glasses at low temperatures. As temperature increases and approaches glass transition temperature T_g, the density of the stable glasses increases more and exceeds that of the ordinary glasses [40].

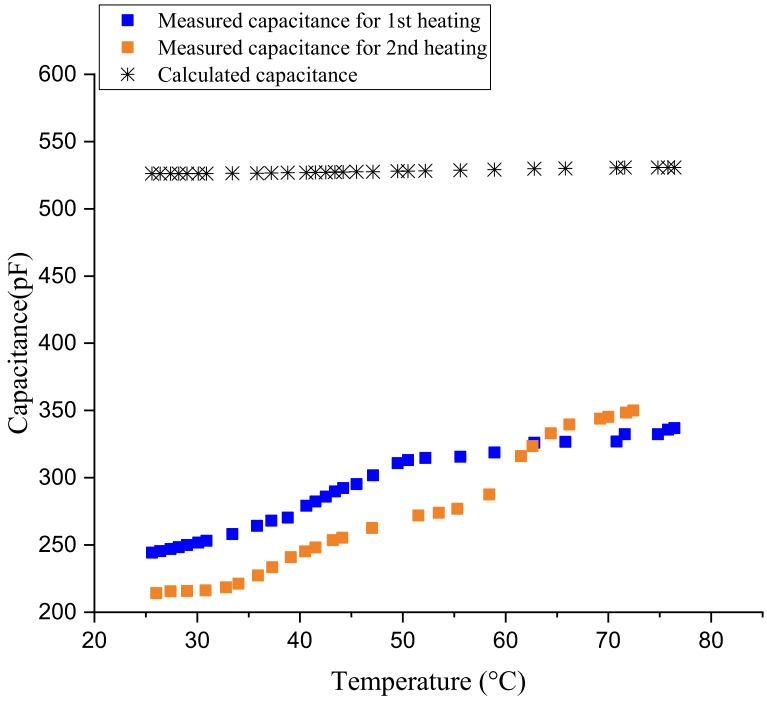

Figure 3.4: Capacitance as a function of temperature for a capacitor filled with two vapor-deposited PMMA films (each has the thickness of around 360 nm) and spacers (5 μm thick). Comparison between measured and calculated capacitances at different temperatures for vapor-deposited PMMA films.

Figure 3.5 shows the measured dielectric loss as a function of temperature for the capacitor filled with vapor-deposited PMMA films. In this figure, the first heating curve represents PMMA vapor-deposited stable glasses, while the second heating curve represents PMMA ordinary glasses. Gaussian fitting has been applied to explore and analyze the dielectric loss curves of the stable glasses and ordinary glasses of PMMA films. The fitting consists of offset and three terms of Gaussian functions. The first Gaussian term represents α relaxation and the second one represents β relaxation and the third one represents

background. The Gaussian fitting equation is expressed by:

$$tan\delta = tan\delta_0 + \frac{A_\alpha}{\sqrt{\pi/2}} e^{-2\frac{(T-T_{c,\alpha})^2}{w_\alpha^2}} + \frac{A_\beta}{\sqrt{\pi/2}} e^{-2\frac{(T-T_{c,\beta})^2}{w_\beta^2}} + A_1 exp(T/b) \tag{3.4}$$

where $tan\delta_0$ is the offset (the sum-up of the lowest $tan\delta$ for α relaxation, β relaxation and background), A represents the amplitude of a relaxation peak, w represents the width of a relaxation peak. x_c represents the center of relaxation peak. Here, the background part can be expressed in the form of Gaussian fitting term because the measured dielectric loss for background in Figure 2.10 can be fitted by using Gaussian equation.

By applying nonlinear curve fitting in Origin software, the optimal solution of each parameter in the equation can be obtained through iteration. The parameter values in the Gaussian fitting functions are given in Table 3.1 and Table 3.2. The terms for different relaxations in the Gaussian fitting functions are indicated by the dashed curves. Based on the fitting results in the tables, it can be seen that the amplitudes of α relaxation for the first heating curve and the second heating curve are slightly different. However, the amplitudes of β relaxation for the first heating curve and the second heating curve are significantly different. In order to compare the β relaxation peaks for stable PMMA glasses with ordinary PMMA glasses, the relative amplitudes of the β relaxation to α relaxation on the first heating curve and the second heating curve need to be investigated. For the stable glasses, its β relaxation amplitude is 12.1 times smaller than its α relaxation amplitude. For the ordinary glasses, its β relaxation amplitude is 3.9 times smaller than its α relaxation amplitude. Therefore, the relative amplitude of β relaxation to the α relaxation for stable PMMA glasses is smaller than that for ordinary PMMA glasses. In the other word, the β relaxation peak for the stable glasses is suppressed compared to the ordinary glasses. The relative β relaxation amplitude ratio of the stable glasses to ordinary

glasses is defined as suppression factor. The suppression factor (x) of β relaxation for the stable glasses can be determined by:

$$\begin{aligned} x &= \frac{(A_\beta/A_\alpha)_{ordinary}}{(A_\beta/A_\alpha)_{stable}} \\ &= \frac{(5.1\times10^{-3}/2.0\times10^{-2})}{(1.4\times10^{-3}/1.7\times10^{-2})} \\ &= 3.1 \end{aligned} \tag{3.5}$$

where A_β is the β relaxation amplitude, A_α is the α relaxation amplitude. From the calculation, we can tell that the relative amplitude of β relaxation to the α relaxation for stable glasses has decreased by 3.1 times compared to that for ordinary glasses after rejuvenation.

This is the first measurement of dielectric relaxations in vapor-deposited stable polymer glasses. Before, there were only the studies of dielectric relaxation in vapor deposited stable glasses of small organic molecules such as toluene and indomethacin. The finding of decrease in β relaxation amplitude in stable polymer glasses is in good agreement with the suppression β relaxation amplitude in the stable glasses of toluene. The suppression factor of β relaxation is slightly smaller than the suppression factor (3.4) for stable glasses of toluene in HB Yu et al [21]. This suppression of β relaxation in PMMA stable glasses results from restricted local motions in the stable glasses with higher density and greater kinetic stability.

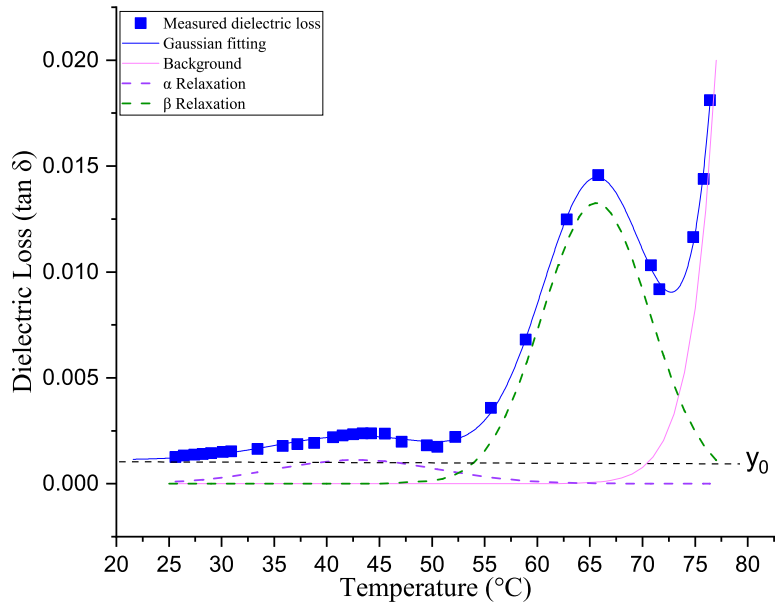

a. first heating

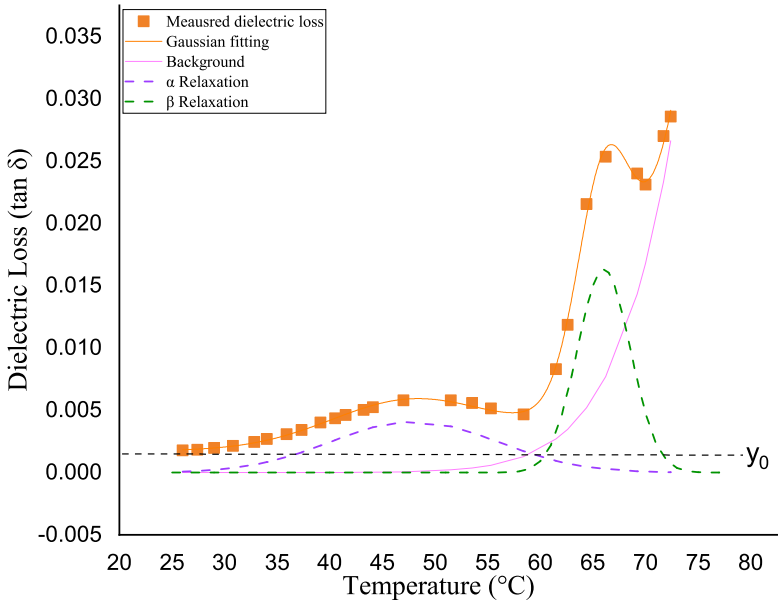

b. second heating

Figure 3.5: Dielectric loss as a function of temperature for two vapor-deposited PMMA films (each has the thickness of around 360 nm) and spacers (5 μm thick). (a) first heating. (b) second heating.

As shown in Figure 3.5.a, β relaxation peak is observed around 43 °C while the peak of the α relaxation is observed at around 66 °C. Figure 3.5.b shows the fitting dielectric curves for the second heating. We can notice that the β relaxation peak for the second heating shows up at approximately 48°C while the α relaxation peak shows up at approximately 66°C. Therefore, the positions of dielectric relaxation peaks for the stable glasses and ordinary glasses of PMMA are the same, suggesting that the molecular weight of the PMMA stable glasses almost maintained the same after heating above T_g and rejuvenating to ordinary glasses.

As mentioned in previous sections, for the same capacitor setting, steps on the capacitance curve can be related to dielectric relaxation peaks on the dielectric loss curve. The first step on the first heating curve is observed at around 50 °C, which is related to β relaxation of the stable glasses. The next step seems to be observed at around 60 °C but it is not sufficiently pronounced. This step is related to α relaxation of the stable glasses. For the second heating, two steps are observed on the capacitance curve for the ordinary glasses. The one at around 50 °C is associated with β relaxation of the ordinary glasses. The other one around 60 °C is associated with α relaxation of the ordinary glasses.

In the dielectric measurements, it is better to have the dielectric curves for the third heating to ensure the results of dielectric measurements on rejuvenated ordinary glasses are reproducible. However, when the third heating was performed, significant drops in capacitance and loss were observed. Also, a variety of colors reflected onto the stable glass films could not be observed any more. The phenomena may be induced by the dewetting process of the PMMA stable glasses with low molecular weights at a temperature higher than T_g. Due to the low viscosity and high mobility of the stable glass of PMMA films at the high temperature, holes may start to form, which results from the rupture of PMMA films. Subsequently, the ruptured films may split into several droplets. The entire process

is called dewetting process [41]. For the first heating and second heating, the maximum temperatures in the dielectric measurements ought not to be higher than 25 °C above the T_g of the stable glass, in case the deposited films may break up and undergo a dewetting process due to the high mobility of the glass. Here we set the maximal temperature up to 75 °C. As soon as the temperature reaches 75 °C, the capacitor should be cooled down immediately to avoid the rupture of the PMMA films caused by the dewetting.

Table 3.1: The results of the fitting to equation 3.4 for stable glass of PMMA films

offset	$tan\delta_0$	$1.1\times10^{-3}\pm1.1\times10^{-4}$
center of α relaxation	$T_{c,\alpha}$	65.6±0.3
width of α relaxation	w_α	10.2±0.4
amplitude of α relaxation	A_α	$1.7\times10^{-2}\pm4.6\times10^{-4}$
center of β relaxation	$T_{c,\beta}$	42.8±0.8
width of β relaxation	w_β	15.5±2.4
amplitude of β relaxation	A_β	$1.4\times10^{-3}\pm1.4\times10^{-4}$
amplitude of background	A_1	$7.4\times10^{-17}\pm9.9\times10^{-18}$
fitting constant of background	b	$2.3\pm8.8\times10^{-3}$

Table 3.2: The results of the fitting to equation 3.4 for ordinary glass of PMMA films after rejuvenation

offset	$tan\delta_0$	$1.8\times10^{-3}\pm3.1\times10^{-4}$
center of α relaxation	$T_{c,\alpha}$	66.0±0.2
width of α relaxation	w_α	5.0±0.4
amplitude of α relaxation	A_α	$2.0\times10^{-2}\pm2.4\times10^{-3}$
center of β relaxation	$T_{c,\beta}$	48.0±1.3
width of β relaxation	w_β	15.7±2.7
amplitude of β relaxation	A_β	$5.1\times10^{-3}\pm5.6\times10^{-4}$
amplitude of background	A_1	$2.1\times10^{-17}\pm3.8\times10^{-18}$
fitting constant of background	b	$2.2\pm1\times10^{-2}$

3.4 Effect of roughness on capacitor plates

As shown in Figure 2.8 and Figure 3.4, the calculated capacitance deviates significantly from the measured capacitance. The calculated capacitance is dependent on the relative permittivity of a dielectric material. However, the measured capacitance does not seem to be dependent on the relative permittivity of dielectric materials. It is postulated that the calculated capacitance differs significantly from the measured capacitance because the actual plate capacitor used in dielectric measurements is not perfectly parallel and smooth. In order to verify this hypothesis, a plausible model for a plate capacitor with roughness needs to be constructed.

A geometry of a plate capacitor with roughness may arise during the polishing process. After being polished with sandpaper/large-particle slurries, the roughness of the disk surface became smaller. After being polished with smallest-particle (0.05 μm) slurries, the disk surface became relatively flat (most part of the disk has a very small roughness of 0.05 μm). Unfortunately, since the polishing was conducted manually, it is hard to ensure that the entire disk has been polished thoroughly and uniformly. Most parts of a polished disk is flat (roughness of around 0.05 μm) while rest part may have a roughness of around 5 μm. Even though the roughness of around 5 μm is small, it may has a huge effect on the capacitance calculation. It is worth noting that when we were doing dielectric measurements, a "high to low short" error was observed at times. The error may be caused by the unevenness of non-parallel capacitor plate surface. In this section, calculations based on a nonparallel capacitor model would explain how the capacitor geometry influences the measured capacitance.

A plate capacitor with roughness of around 5 μm partially filled with one PMMA film is illustrated in Figure 3.6. From previous calculations, it was found that the Teflon spacers

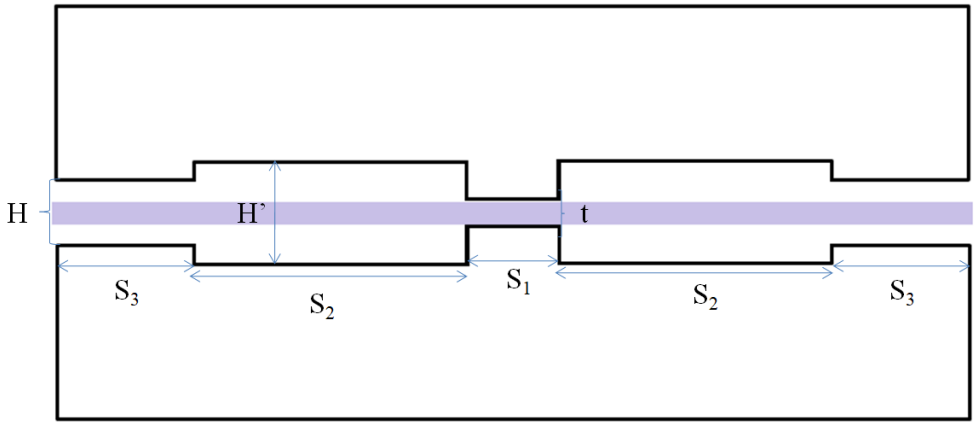

Figure 3.6: The illustration of the plate capacitor (with roughness of $5\mu m$) partially filled with PMMA film. The center part has the surface area of S_1 and the spacing of t (t is also the thickness of the PMMA film). The periphery part has the surface area S_3 and the spacing of H. The middle part between the two has the surface area S_2 and the spacing of $H^{'}$.

have almost no effect on the total capacitance. Hence, the capacitance of the part filled with spacers is negligible in this new model. Also, the effect of films' thermal expansion can be neglected so the increased thicknesses of the PMMA film and the spacers are not taken into consideration in the new model.

The capacitance of a perfectly smooth plate capacitor, which is partially filled PMMA, can be expressed by:

$$\begin{aligned} C &= \frac{1}{\frac{1}{C_{PMMA}} + \frac{1}{C_{air}}} \\ &= \frac{1}{\frac{H-t}{\varepsilon_0 S} + \frac{t}{\varepsilon_0 \varepsilon_r' S}} \\ &= \frac{\varepsilon_0 S}{H - t/(1 - 1/\varepsilon_r')} \\ &= \frac{\varepsilon_0 S}{H} \frac{1}{1 - t/H(1 - 1/\varepsilon_r')} \end{aligned} \tag{3.6}$$

where S is the surface area of PMMA film, H is the spacing between two plates, t is the

film thickness.

As shown in Figure 3.6, this capacitor with a symmetric geometry has three parts because of its roughness. The center part has the surface area of S_1 and the spacing of t. This part is fully filled with PMMA. The outer part has the surface area S_2 and the spacing of $H^{'}$. The outermost part has the surface area S_3 and the spacing of H. H is the sum-up of the PMMA film thickness and the spacer thickness. In this case, the capacitance for the center part is given by:

$$\begin{aligned} C &= \frac{\varepsilon_0 S_1}{t} \frac{1}{1 - t/t(1 - 1/\varepsilon_r^{'})} \\ &= \frac{\varepsilon_0 S_1 \varepsilon_r^{'}}{t} \end{aligned} \tag{3.7}$$

For the capacitor partially filled with one dropcoated PMMA film, the total capacitance is given by:

$$C_{total} = \frac{\varepsilon_0 S_1 \varepsilon_r^{'}}{t} + \frac{\varepsilon_0 S_2}{H'} \frac{1}{(1 - t/H'(1 - 1/\varepsilon_r^{'}))} + \frac{\varepsilon_0 S_3}{H} \frac{1}{(1 - t/H(1 - 1/\varepsilon_r^{'}))} \tag{3.8}$$

We assume that $S{=}\pi r^2$ ($r = 0.95$ cm), $S_1 = 0.04S$, $S_2 {=} 0.7S$, $S_3 = 0.26S$, $t = 2.9$ μm, $H^{'} = 12$ μm, $H = 7.9$ μm. Figure 3.7 shows the calculated capacitance at different temperatures for this capacitor with roughness of 5μm. It can be seen that, if such a capacitor model with roughness is applied, its capacitance values will increase by 22% when ε_r changes from 2.9 to 4.9. This increased percentage of 22% is close to that of the measured capacitance (which is 19%) compared to that of the previously-calculated capacitance (which is 6%) . Compared to the calculated capacitance for a parallel capacitor, the calculated capacitance for a capacitor with roughness is in better agreement with the measured capacitance.

For the capacitor partially filled with two vapor-deposited PMMA film, The outer-

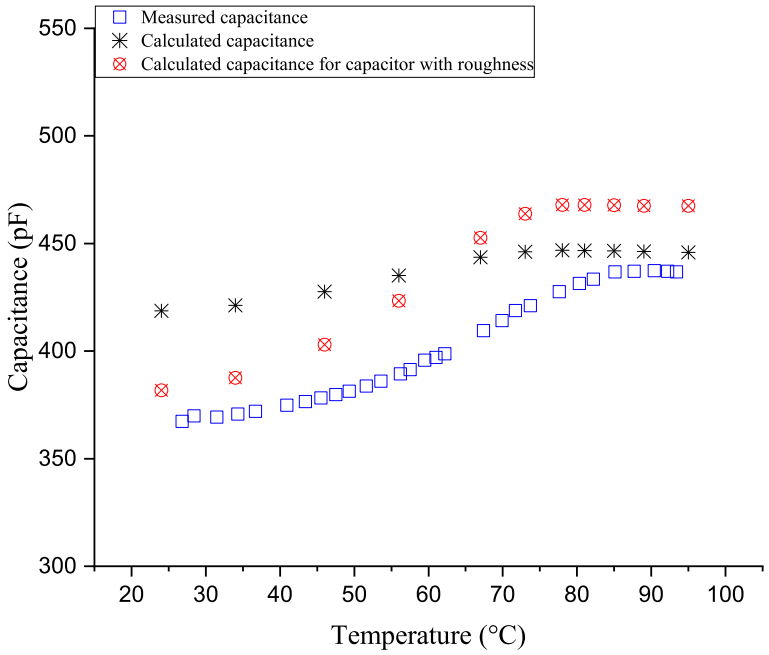

Figure 3.7: Comparison of the calculated capacitance values between the smooth plate capacitor model and the plate capacitor model with roughness of around 5μm. The capacitor is partially filled with a dropcoated PMMA film.

most part (0.65 cm<R<0.95 cm) filled with spacers has the spacing of 5μm. We assume that S_{PMMA}=πr_{PMMA}^2 (r_{PMMA} = 0.65cm), S_1 = 0.03S_{PMMA}, S_2 =0.95S_{PMMA}, S_3 = 0.02S_{PMMA}, t =2×d_{PMMA} = 720 nm (d_{PMMA} is the thickness of one vapor-deposited PMMA film), $H^{'}$ = 10 μm, H = 5 μm. The capacitance around the edge (with H = 5 μm) is given by:

$$\begin{aligned} C_{edge} &= \frac{1}{1/C_{PMMA} + 1/C_{air}} \\ &= \frac{1}{t/\varepsilon_0\varepsilon_r^{'}S_3 + (H-t)/\varepsilon_0 S_{air}} \end{aligned} \tag{3.9}$$

where S_{air}=$S_3 + \pi r^2 - \pi r_{PMMA}^2$ (r=0.95cm, r_{PMMA}=0.65cm).

The total capacitance is given by:

$$C_{total} = \frac{\varepsilon_0 S_1 \varepsilon_r^{'}}{t} + \frac{\varepsilon_0 S_2}{H^{'}} \frac{1}{(1 - t/H^{'}(1 - 1/\varepsilon_r^{'}))} + C_{edge} \tag{3.10}$$

The calculated capacitance for this capacitor (with roughness of $5\mu m$) partially filled with vapor-deposited PMMA films is shown in Figure 3.8. It can be observed that the calculated capacitance for the capacitor model with roughness of is in better agreement with the measured capacitance as compared to that for the smooth capacitor model. When such a capacitor model with roughness is applied, its capacitance values will increase by 39% when $\varepsilon_r^{'}$ changes from 2.9 to 4.9. This increased percentage of 39% is close to that for the measured capacitance on the first heating curve (which is 39% as well).

From a series of calculations, it has been verified that this plausible model of a non-parallel plate capacitor (Figure 3.6) is the reason for the deviation shown in Figure 2.8 and Figure 3.4. The model has been applied in the calculations for a capacitor filled with dropcoated PMMA and a capacitor filled with deposited PMMA. The calculated results show that the calculated capacitance values for this new model are in better agreement with that for measured capacitance values compared to that for the ideal smooth capacitor plate model. It implies that, other than dielectric material, the geometry of a plate capacitor is also an essential factor which has a huge impact on the measured capacitance.

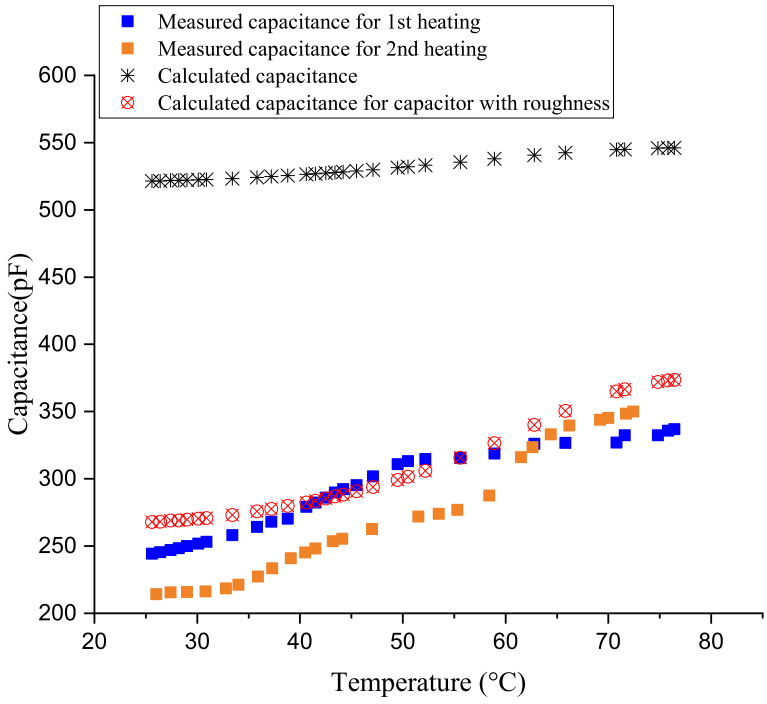

Figure 3.8: Comparison of the calculated capacitance values between the smooth plate capacitor model and the plate capacitor model with roughness of around 5μm. The capacitor is partially filled with two vapor-deposited PMMA films.

Concluding remarks and future work

In conclusion, dielectric measurements have been conducted on the ordinary glasses and vapor-deposited glasses of PMMA in an attempt to study the effect of glass stability on the β dielectric relaxation. To yield a highly monodisperse PMMA sample, fractional distillation was used for separating different components of a PMMA sample. Subsequently, PVD was used for depositing stable glass of PMMA on electrodes. Based on the dielectric loss values of ordinary glass and of stable glass collected from capacitance bridge, it can be observed that there is a noticeable suppression on the β relaxation peak for stable PMMA glasses compared to that for ordinary PMMA glasses. The relaxation amplitude parameters obtained from Gaussian fitting tell us that the suppression factor turns out to be 3.1. The suppression arises from a more efficient molecular packing and hindered local motions of the stable polymer chains. Therefore, the enhanced stability in polymer stable glasses essentially leads to the decrease in its β relaxation amplitude.

Not only dielectric loss but also capacitance has been obtained by dielectric measurements. For the same capacitor geometry, the steps on the capacitance curve are related to relaxation peaks on the dielectric loss curve. It is found that the capacitance values, calculated by using a parallel and smooth plate capacitor model, deviate significantly from the experimental results. However, the capacitance values, calculated by using a plate capacitor model with roughness of $5\mu m$, are in great agreement with the measured capac-

itance. This finding implies that the capacitance is very sensitive to any change in the dielectric material of the capacitor.

There are still many challenges in the project. When the heating rate is very fast, it is difficult to ensure that the reached maximum temperature in each temperature scan cycle is in the appropriate range. A too high temperature most likely leads to severe dewetting, while a too low temperature may lead to incomplete rejuvenation. After several temperature scan cycles, we noticed decreases in both capacitance and dielectric loss values, possibly resulting from the too high temperatures. In addition, the actual capacitor plates we used are not perfectly smooth can also also an issue. Although we can build a feasible model to analyze the effect of capacitor plates with roughness on the experimental results, there is still difference between the geometry of the built model and that of the actual plates.

For future work, deposition rates and substrate temperatures can be adjusted to change the physical properties of stable glass of polymers. The change in stable glass density may have an effect on how it behaves and rejuvenates at a high temperature. Optimizing the deposition rate and substrate temperature may contribute to conducting more cycles of temperature scans on the stable glass and ordinary glass of PMMA films. Also, the material of capacitor electrodes can be replaced with metal of smooth surface and good conductivity (such as gold). Furthermore, other kinds of polymeric glasses can be used in the dielectric measurements. By testing other polymer glasses, it can be further confirmed that the increase in polymer glass stability can lead to greater suppression of β relaxation.

References

[1] R Casalini, D Fragiadakis, and CM Roland. Relaxation dynamics of poly (methyl acrylate) at elevated pressure. *Macromolecules*, 44(17):6928–6934, 2011. viii, 4

[2] Norman Gerard McCrum, Bryan Eric Read, and Graham Williams. Anelastic and dielectric effects in polymeric solids. 1967. viii, 6, 16

[3] Mark D Ediger. Perspective: Highly stable vapor-deposited glasses. *The Journal of chemical physics*, 147(21):210901, 2017. viii, 9, 11

[4] Heedong Yoon, Yung P Koh, Sindee L Simon, and Gregory B McKenna. An ultrastable polymeric glass: Amorphous fluoropolymer with extreme fictive temperature reduction by vacuum pyrolysis. *Macromolecules*, 50(11):4562–4574, 2017. viii, 10, 12

[5] Hiroaki Usui. Preparation of polymer thin films by physical vapor deposition. *Functional Polymer Films: 2 Volume Set*, pages 287–318, 2011. ix, 36, 37

[6] Adam N Raegen, Junjie Yin, Qi Zhou, and James A Forrest. Ultrastable monodisperse polymer glass formed by physical vapour deposition. *Nature Materials*, 19(10):1110–1113, 2020. x, 38, 42

[7] WV Metanomski. *Compendium of macromolecular nomenclature*. Blackwell Scientific Publications, 1991. 1

[8] Robert J Young and Peter A Lovell. *Introduction to polymers*. CRC press, 2011. 1

[9] M Rubinstein and RH Colby. Polymer physics, oxford university press. *New York.[Google Scholar]*, 2003. 1

[10] Neil A Dotson, Rafael Galvan, Robert L Laurence, and Matthew Tirrell. *Polymerization process modeling*. John Wiley Sons, 1995. 2

[11] ULF Gedde. *Polymer physics*. Springer Science Business Media, 1995. 2

[12] Bhawani Chowdhry and JE Brignell. *Dielectric Relaxation and Measurement Methods*. 1991. 3

[13] HLJ Eliasson. Relaxation processes in disordered systems: Dielectric studies of amorphous and semicrystalline polymers. 2001. 4

[14] Thomas G Fox Jr and Paul J Flory. Second-order transition temperatures and related properties of polystyrene. i. influence of molecular weight. *Journal of Applied Physics*, 21(6):581–591, 1950. 5

[15] R Bergman, F Alvarez, A Alegrıa, and J Colmenero. The merging of the dielectric α-and β-relaxations in poly-(methyl methacrylate). *The Journal of chemical physics*, 109(17):7546–7555, 1998. 5, 24

[16] JMG Cown. Some general features of tg-m relations for oligomers and amorphous polymers. *European Polymer Journal*, 11(4):297–300, 1975. 7

[17] Leendert Cornelis Elisa Struik. Physical aging in amorphous polymers and other materials. 1977. 8

[18] Gregory B McKenna. On the physics required for prediction of long term performance of polymers and their composites. *JOURNAL OF RESEARCH-NATIONAL INSTITUTE OF STANDARDS AND TECHNOLOGY*, 99:169–169, 1994. 8

[19] Gregory B McKenna. Physical aging in glasses and composites. In *Long-term durability of polymeric matrix composites*, pages 237–309. Springer, 2012. 9

[20] Sadanand Singh, Mark D Ediger, and Juan J De Pablo. Ultrastable glasses from in silico vapour deposition. *Nature materials*, 12(2):139–144, 2013. 10

[21] HB Yu, M Tylinski, Anthony Guiseppi-Elie, MD Ediger, and Ranko Richert. Suppression of β relaxation in vapor-deposited ultrastable glasses. *Physical review letters*, 115(18):185501, 2015. 10, 45

[22] Stephen F Swallen, Kenneth L Kearns, Marie K Mapes, Yong Seol Kim, Robert J McMahon, Mark D Ediger, Tian Wu, Lian Yu, and Sushil Satija. Organic glasses with exceptional thermodynamic and kinetic stability. *Science*, 315(5810):353–356, 2007. 10

[23] Shakeel S Dalal, Zahra Fakhraai, and Mark D Ediger. High-throughput ellipsometric characterization of vapor-deposited indomethacin glasses. *The Journal of Physical Chemistry B*, 117(49):15415–15425, 2013. 10

[24] KL Ngai, Marian Paluch, and Cristian Rodríguez-Tinoco. Why is the change of the johari–goldstein -relaxation time by densification in ultrastable glass minor? *Physical Chemistry Chemical Physics*, 20(43):27342–27349, 2018. 12, 13

[25] HB Yu, M Tylinski, Anthony Guiseppi-Elie, MD Ediger, and Ranko Richert. Suppression of relaxation in vapor-deposited ultrastable glasses. *Physical review letters*, 115(18):185501, 2015. 12

[26] Graham Williams. Molecular aspects of the dielectric relaxation of solid polymers. In *Conference on Electrical Insulation & Dielectric Phenomena-Annual Report 1982*, pages 3–28. IEEE, 1982. 13

[27] M Vogel and E Rössler. Slow β process in simple organic glass formers studied by one and two-dimensional 2 h nuclear magnetic resonance. ii. discussion of motional models. *The Journal of Chemical Physics*, 115(23):10883–10891, 2001. 13

[28] M Vogel and E Rössler. Slow β process in simple organic glass formers studied by one-and two-dimensional 2 h nuclear magnetic resonance. i. *The Journal of Chemical Physics*, 114(13):5802–5815, 2001. 13

[29] Bhawani Chowdhry and JE Brignell. *Dielectric Relaxation and Measurement Methods*. 1991. 15

[30] Mikiko Shima, Mari Sato, Miharu Atsumi, and Koichi Hatada. Dipole moments of isotactic and syndiotactic poly (methyl methacrylate) and their temperature dependence. *Polymer journal*, 26(5):579–585, 1994. 16

[31] RM Hill and LA Dissado. Debye and non-debye relaxation. *Journal of Physics C: Solid State Physics*, 18(19):3829, 1985. 16

[32] Vera V Daniel. *Dielectric relaxation*. Academic press, 1967. 16

[33] R Casalini, CM Roland, and Simone Capaccioli. Effect of chain length on fragility and thermodynamic scaling of the local segmental dynamics in poly (methylmethacrylate). *The Journal of chemical physics*, 126(18):184903, 2007. 17

[34] Shipei Zhu. Production of highly monodisperse polystyrene by evaporative purification. Master's thesis, University of Waterloo, 2017. 35

[35] PP Luff and M White. The structure and properties of evaporated polyethylene thin films. *Thin solid films*, 6(3):175–195, 1970. 36

[36] Akiyoshi Takeno, Norimasa Okui, Tetsuji Kitoh, Michiharu Muraoka, Susumu Umemoto, and Tetsuya Sakai. Preparation and piezoelectricity of β form poly (vinylidene fluoride) thin film by vapour deposition. *Thin Solid Films*, 202(2):205–211, 1991. 36

[37] R Chow, MK Spragge, GE Loomis, F Rainer, RL Ward, IM Thomas, and MR Kozlowski. Characterization of physically vapor deposited af2400 thin films. *MRS Online Proceedings Library (OPL)*, 328, 1993. 36

[38] Rybka V. Efmenko K. Hnatowicz V. Svorcik, V. Deposition of polystyrene films by vacuum evaporation. *J. Mat. Sci. Lett. 16, 1564–1566*, page 1564–1566, 1997. 36

[39] Michael Wübbenhorst, Angeline Kasina, Simona Capponi, Bram Vanroy, and Simone Napolitano. Ultrathin polymer films by single molecule deposition. *Journal of Non-Crystalline Solids*, 407:270–276, 2015. 38

[40] Shakeel S Dalal and Mark D Ediger. Molecular orientation in stable glasses of indomethacin. *The journal of physical chemistry letters*, 3(10):1229–1233, 2012. 42

[41] Ioannis Karapanagiotis and William W Gerberich. Polymer film rupturing in comparison with leveling and dewetting. *Surface science*, 594(1-3):192–202, 2005. 48